

Maintenance of the Intertropical Convergence Zones and the Large-Scale Tropical Circulation on a Water-covered Earth

PETER G. HESS

National Center for Atmospheric Research, Boulder, Colorado

DAVID S. BATTISTI

Department of Atmospheric Sciences, University of Washington, Seattle, Washington

PHILIP J. RASCH

National Center for Atmospheric Research, Boulder, Colorado

(Manuscript received 7 May 1991, in final form 12 May 1992)

ABSTRACT

How the surface boundary heating (sea surface temperature) and cumulus adjustment process affect the location, structure, energetics, and dynamics of the intertropical convergence zones (ITCZs) is investigated. A series of experiments is performed with a general circulation model where the lower boundary is specified to be water at a fixed sea surface temperature (SST), an aqua planet. All experiments are run using equinoctial insolation with no longitudinal variation in SST. Two different convective parameterization schemes (Kuo and moist convective adjustment) and several different zonally symmetric SST distributions are used in these experiments.

The location of the ITCZ is found to be sensitive to the convective parameterization scheme and the SST distribution. The model with the moist convective adjustment scheme produces an ITCZ over the tropical SST maximum, even under conditions where the SST gradient is weak. By contrast, the model with the Kuo convective parameterization is not as sensitive to SST distribution: the model with the Kuo scheme yields two ITCZs straddling the equator at approximately 7° latitude for a wide variety of SST distributions, including when the warmest water is located on the equator. The location of the ITCZ affects the structure and strength of both the time-mean Hadley cells and the subtropical jets. Furthermore, the equatorial wave spectrum is strongly influenced by the type of cumulus parameterization scheme used. The "convective characteristics" for each parameterization scheme are presented in detail to elucidate the influence of the large-scale environment on convection.

1. Introduction

The intertropical convergence zones (ITCZs) are prominent features of the earth's atmosphere. They appear in satellite photographs as bands of clouds on the order of a few degrees of latitude in width, roughly aligned in the east–west direction. Over land the ITCZs tend to follow the seasonal march of the sun. Over the Pacific Ocean, however, there is a distinct precipitation minimum over the equator during all seasons (Taylor 1973; Jaeger 1976) with the ITCZ generally located north of the equator. There is a slight tendency for two off-equatorial ITCZs to form over the eastern Pacific Ocean in boreal spring. The ITCZ constitutes the upward branch of the large-scale meridional Hadley circulation through which the midlatitudes are directly linked to the tropics. The thermally direct Hadley cir-

ulation must exist within the latitudes where there is insufficient angular momentum provided by the curvature of the earth to balance a radiative equilibrium wind profile (Schneider 1977, 1984; Held and Hou 1980; Dunkerton 1989). Moreover, in a moist atmosphere the upward branch of the Hadley cell should manifest itself as a thin zone of cumulus towers—the ITCZ.

There is a propensity for the observed ITCZ to occur over the warmest sea surface temperature (SST) (Fig. 1; see also Saha 1971). In Fig. 1 we have displayed the "meridional sea surface temperature differences" (SSTD) across the equatorial Pacific Ocean for the March–May season, with the location of the climatological maximum in rainfall (i.e., the ITCZ) superimposed. Here, SSTD is defined as the difference between the SST and SST on the equator along the same meridian. Thus, the SSTD indicates the strength and direction of the (dominant) meridional SST gradient averaged between any location and the equator. Neg-

Corresponding author address: David Battisti, Dept. of Atmospheric Sciences, University of Washington, Seattle, WA 98195.

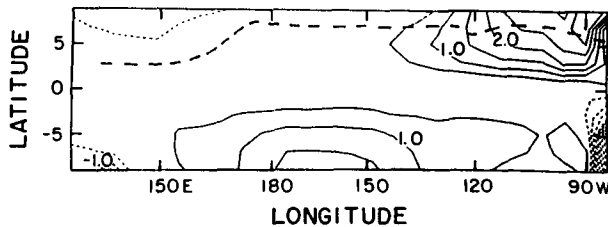


FIG. 1. A contour plot of the equatorial Pacific Ocean “meridional sea surface temperature differences” (SSTD) across the equatorial Pacific Ocean for the March–May season (see text). The location of the climatological maximum in rainfall (i.e., the ITCZ) for March–May is indicated by a heavy dashed line. The plot is produced using the monthly averaged SST from COADS and the precipitation estimates from Dorman and Bourke (1979). The contour interval is 0.5°C and positive (negative) contours are solid (dashed).

ative SSTD values flanking the equator indicate a SST maximum near the equator, while positive values north of the equator in conjunction with negative values south of the equator indicate a “large-scale” meridional SST gradient with warmer water north of the equator and colder water south of the equator. A careful examination of the observations plotted in Fig. 1 indicates that it is not solely the SST that determines the position of the ITCZ. In the Pacific the ITCZ tends to be located in the Northern Hemisphere even when the highest SSTs are situated south of the equator. Additionally, there is a rather large area in the central Pacific where the SST gradients are weak, yet the ITCZ is found well to the north of the equator (Fig. 1). Also, note that in the western Pacific the SST is a maximum on the equator, yet the maximum in precipitation is still sharply confined and is located off the equator (see also Jaeger 1976).

The axisymmetric model studies of Pike (1971), Schneider (1977), and Goswami et al. (1984) produce precipitation maxima over the warmest water. Pike’s study is unique in that the axially symmetric atmospheric model is coupled to an axially symmetric ocean model, whereby cold water is upwelled along the equator and the ITCZ is forced off the equator. Neelin and Held (1987) develop a simple atmospheric model for the low-level convergence based on the moist static energy balance. In this model the low-level convergence is directly related to SSTs, with maximum convergence (precipitation) occurring over the warmest water. The meridional spatial scales for the precipitation are much larger than those observed, however, especially in the western Pacific where the SST gradients are generally small.

The studies of Charney (1966) and Holton et al. (1971) suggest that off-equatorial ITCZs may exist with maximum SST on the equator due to processes inherent to the atmosphere. Charney (1966, 1971) theorizes that the structure and dynamics of the ITCZs are governed by conditional instability of the second kind (CISK), where moisture convergence is maintained

by boundary-layer pumping. Charney argues that the position of the ITCZ is determined by a balance between the supply of moist static energy, decreasing from the equator to the pole, and boundary-layer convergence that increases with the Coriolis parameter; however, Charney’s hypothesis is questioned by Schneider and Lindzen (1977).

Holton et al. (1971) argue that zonally propagating equatorial waves may help to organize convective activity off the equator in the tropics (wave-CISK) through a singularity in the (Ekman) boundary-layer equations and, hence, may significantly contribute to the time-mean convection (the ITCZ). The maximum boundary-layer convergence associated with these waves occurs at the critical latitude where the local Coriolis frequency equals the frequency of the wave. The authors in this study note that the 4–5 day easterly waves observed in the tropical eastern Pacific (Wallace and Chang 1969) should achieve maximum fueling from wave-CISK at a critical latitude of about 6° and, in a time average, be manifest as an ITCZ (or, in an axially symmetric atmosphere, two ITCZs paralleling the equator at about 6° latitude). Chang (1973) shows that the critical latitude argument holds for a finite-depth boundary layer. While Holton et al. (1971) suggest the observed off-equatorial ITCZ in the Pacific may be wave induced, they point out that the cause and effect is not clear. Charney (1973), on the other hand, suggests it is a preexisting ITCZ that sets the vertical and horizontal scales of the waves.

Recently, the question of what determines the position of the ITCZ has resurfaced in connection with atmospheric models. Hayashi and Sumi (1986) run a general circulation model (GCM) with the lower boundary condition set to a global ocean surface (an aqua planet) with zonally and hemispherically symmetric sea surface temperatures monotonically decreasing from the equator. They find two ITCZs straddling the equator even though the SST maximum is prescribed to be on the equator. Swinbank et al. (1988) repeat Hayashi and Sumi’s aqua planet experiment using the European Centre for Medium-Range Forecasts (ECMWF) GCM and also report twin ITCZs flanking the equator. Lau et al. (1988), however, in a similar aqua planet experiment with the GFDL GCM, find one ITCZ on the equator. In their case, the sea surface temperature is determined by the condition that there is no net averaged energy flux through the lower boundary. Lau et al. (1988, appendix A) suggest that their aqua planet climatology differs from that in Hayashi and Sumi (1986) and Swinbank et al. (1988) because of the differences in surface energy fluxes that arise from the different SST boundary conditions.

Thus, over an ocean with SST maximized on the equator there still seems to be some question as to whether the atmosphere favors a single ITCZ centered on the equator, as suggested by the axisymmetric theory and calculations, or two ITCZs paralleling the equator,

as Charney (1966) and Holton et al. (1971) suggest. We have run a set of experiments with a GCM in an aqua-planet configuration to examine the processes that determine the position and maintenance of the ITCZ. We choose an aqua planet configuration so as to avoid the complicating effects of orography and landmass heating on the location of the ITCZs. Furthermore, the SST is zonally symmetric, eliminating the possible effect of time-mean zonally asymmetric circulations on the position of the ITCZ. The effect of zonal asymmetries is currently being studied. With one exception, the set of experiments described in this paper features changes only in the prescribed SST and the parameterization scheme for convection. The maximum solar radiation is directly over the equator in perpetual 21 March conditions in all experiments.

The paper is organized as follows. In section 2 we give a brief description of the general circulation model used and the convective parameterization schemes implemented in it. We summarize in section 3 the various experiments and the distinguishing characteristics of each experiment. Two experiments are compared, in some detail, using the "standard" SST distribution but different convective schemes. We isolate the differences between the convective schemes by discussing their "convective characteristics" in section 4, and in section 5 the effect of the two convective parameterizations on zonally asymmetric motions is explored. The effect of the location of the ITCZ on the large-scale circulation is discussed in section 6, and we present the conclusions and a discussion in section 7.

2. The general circulation model

a. Description of the model

For this study of the ITCZ we use version one of the National Center for Atmospheric Research Community Climate Model (CCM1) (Williamson et al. 1987; Hack et al. 1989; hereafter CCM). The simulations are carried out at T42 resolution, using an approximately 2.8 degree Gaussian grid, with 12 unequally spaced vertical levels. The sigma values of the 12 levels are 0.991, 0.926, 0.811, 0.664, 0.500, 0.355, 0.245, 0.165, 0.110, 0.060, 0.025, and 0.009. The standard model contains a convective adjustment parameterization following Manabe et al. (1965) and large-scale stable condensation. No diurnal cycle is used. Simple bulk aerodynamic parameterizations of surface exchange and subgrid-scale vertical diffusion are included (Deardorff 1972). Radiatively active clouds are formed that depend upon the characteristics of the convective processes and large-scale condensation to define the location, depth, and some of the optical properties of the cloud.

We have modified the standard version of the CCM to make an aqua-planet version by modifying the surface boundary condition to an all-ocean surface. The

solar radiative fluxes are fixed at the 21 March values and, for some experiments, we have replaced the standard convection scheme with a Kuo-style scheme discussed below.

b. Description of the convective schemes

The following experiments parameterize convection with either the moist convective adjustment (MCA) scheme or a modified Kuo scheme. The MCA scheme used in the CCM is described in Williamson et al. (1987) and is after the work of Manabe et al. (1965). Essentially this scheme adjusts a saturated, unstable column of air to the moist-adiabatic lapse rate, conserving moist static energy. Relative humidities that exceed saturation due to convective adjustment are adjusted to 100% with the excess water vapor instantly rained out.

The other parameterization for convection used in our experiments is derived from Kuo (1965, 1974), Anthes (1977), Donner et al. (1982), Donner (1986), and Krishnamurti et al. (1983). Briefly, the precipitation is assumed to be proportional to the moisture convergence in the column. A simple "plume type" steady-state cloud model predicts in-cloud properties and mass fluxes. The closure assumptions of the parameterization determine the rainfall rate within the grid box (determined by the "b" parameter). The plume model also predicts a rainfall rate (determined by a Kessler-type microphysical parameterization). The ratio of the two rainfall rates is assumed to define the fractional area occupied by the clouds within the grid box. Nonhydrostatic effects and pressure differences between cloud and environment are incorporated in the present scheme following Donner (1986). The closure assumptions for the b parameter suggested by Krishnamurti et al. (1983) are used. The parameterization scheme yields moisture and heat tendencies for the grid box by cloud transport and condensation processes.

For the purpose of later discussion, it is useful to enumerate the tests made on the large-scale properties of an air column by the Kuo scheme to determine if convection is allowed. These are as follows: 1) a lifting condensation level must exist below 500 mb; 2) conditional instability must exist within the column; 3) the column-mean relative humidity must exceed 50%; 4) there is a convergence of moisture into the column from horizontal transport and surface fluxes; and 5) the vertical velocity must be positive below the lifting condensation level. When all these tests are satisfied, the vertical profile of temperature and moisture is passed to the plume model, which computes in-cloud properties. If the cloud is diagnosed to be more than 200 mb deep and to precipitate, then the closure calculations are performed and grid-scale tendencies associated with phase change and cloud transport are calculated.

TABLE 1. Summary of experiments discussed in this paper.

A summary of the nomenclature for each of the 11 experiments performed. Each experiment in the matrix is identified by the type of convective scheme (prefix) and the lower boundary sea surface temperature condition (suffix). Two convective schemes are used: Kuo and moist convective adjustment. These are denoted by the prefix "Kuo" and "MCA," respectively. The two experiments "Kuo90" and "KuoNwv" are variations on the standard Kuo experiments (see section 3a). Blank matrix elements indicate experiments that were not performed.

A variety of zonally symmetric sea surface temperature distributions are prescribed. These sea surface temperature (SST) distributions are shown schematically below, and plotted for some of the cases in Fig. 2a. The SST distributions are summarized here: Std: The standard SST distribution. SST is symmetric about the equator with maximum SST on the equator. This distribution is the observed SST distribution for 21 March, zonally averaged and symmetrized about the equator. Peq: A strongly peaked symmetric SST distribution, with a marked maximum SST on the equator. The maximum SST is as in the standard case. Poeq: As in the Peq case but with the peak in the SST located in the Northern Hemisphere. Flat: Constant SST equatorward of 30° with a value equal to the SST on the equator from the standard SST profile. Feb 1: SST is asymmetric about the equator with maximum temperature in the Southern Hemisphere. It is representative of the climatological February temperatures in the central Pacific. Feb 2: SST is similar to the Feb 1 distribution but the equatorial asymmetry has been further emphasized: the maximum SST is greater than that in the Feb 1 case. Oct: The SST is the symmetrized climatological October SSTs from the central Pacific, which features a SST minimum on the equator.

Scheme for Convection ↓	Sea Surface Temperature												
	Flat	Std	Oct	Feb 1	Feb 2	Peq	Poeq						
Kuo	Kuo - Flat	Kuo - Std	Kuo - Oct	Kuo - Feb 1	Kuo - Feb 2	Kuo - Peq	Kuo - Poeq						
Kuo													
Kuo90								KuoNwv-Std					
								Kuo90 - Std					
MCA	MCA - Std		MCA - Oct										
Schematic of Each Meridional SST Distribution →													

3. Experiments and results

a. Description of the experiments and summary of the results

This section briefly describes the 11 experiments performed to ascertain the sensitivity of the position of the ITCZ to the SST and the convective parameterization scheme. The experiments, summarized in Table 1, are labeled by the type of convective scheme (MCA or Kuo) and then by one of seven different zonally symmetric SST distributions: all experiments are performed with perpetual equinoctial (21 March) insolation. We will refer to a standard SST distribution (Std) as the observed zonally averaged SST for 21 March, symmetrized about the equator, with the SST modified near the poles so temperatures remain above freezing. A description and schematic representation of the different SST distributions used are given with Table 1. In Fig. 2a we show the SST distributions for the standard experiments, the climatological October distribution (Oct), the February distribution (Feb2) and the equatorially peaked distribution (Peq). A de-

tailed comparison of the standard experiments using the different convective schemes (Kuo-Std and MCA-Std) is given in section 3b.

Two special experiments are performed, labeled as Kuo90-Std and KuoNwv-Std. In Kuo90-Std the relative humidity criterion in the Kuo scheme (condition 3, section 2b) is changed to 90%, while KuoNwv-Std uses the Kuo scheme in a zonally symmetric configuration so that no zonally asymmetric waves are present.

Each of the 11 experiments is run for at least 80 days with the standard experiments run for at least 120 days; only the last 60 days are used in all the time averages. Initial conditions are taken from an arbitrary day of a prior integration in a statistical steady state. It usually takes less than ten days for the ITCZs to adjust to either a new SST distribution or a new convective parameterization scheme. Sharp ITCZs form in each experiment, demonstrating that intense convergence zones are a robust feature of the earth's circulation. Selected time- and zonal-mean circulation statistics are presented in Table 2. The most striking results from the experiments documented in Table 2 are as follows:

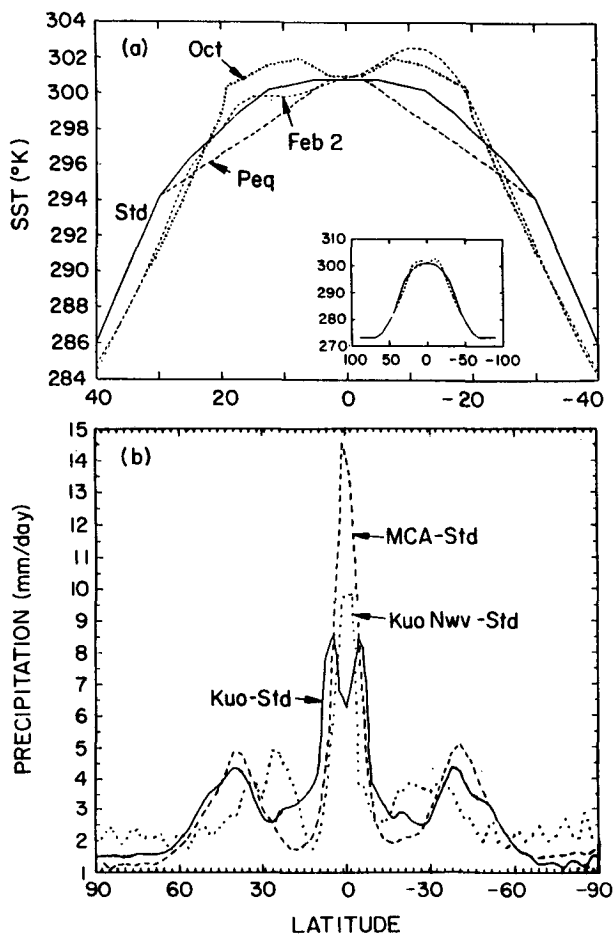


FIG. 2. (a) The prescribed meridional distribution of sea surface temperature vs latitude for the "standard" experiments discussed in this paper ("Std," solid line). The February ("Feb2," short dashed line), October ("Oct," dotted line), and peaked ("Peq," long dashed line) sea surface temperature distributions are also shown. (b) The meridional distribution of zonally averaged precipitation vs latitude for selected experiments (mm day^{-1}): Kuo-Std (solid line), MCA-Std (dashed line), and KuoNwv-Std (dotted line) (see text). In each case the average is taken over a 60-day period after a minimum of 20 days' spinup.

(i) A single general circulation model with identical forcing and boundary conditions yields a tropical circulation that is *qualitatively* changed by changing only the parameterization of convection in the model (Kuo-Std and MCA-Std).

(ii) The model with a Kuo scheme produces two off-equatorial ITCZs with a SST distribution that maximizes on the equator (Kuo-Std) or with SST uniform in the tropics (Kuo-Flat).

The propensity for the Kuo scheme to form two ITCZs is apparent even with the heightened asymmetric February SST boundary conditions (Kuo-Feb2; see Table 2 and Fig. 2a). The CCM with the Kuo scheme does give a single convergence zone when the SST is sharply peaked (Kuo-Peq, Kuo-Poeq) or the

relative humidity criterion (condition 3, section 2b) is changed to 90% (Kuo90-Std). We will for the moment concentrate on the differences between Kuo-Std and MCA-Std experiments.¹

b. Comparison of the standard experiments

The zonal- and time-averaged daily rainfall from the model runs with the standard SST distribution and either the MCA or Kuo convective parameterizations is shown in Fig. 2b. We note that the equatorial ITCZ in the MCA-Std case has significantly more rainfall than the off-equatorial ITCZ in the Kuo-Std case. Figure 3 shows the power of 12-hour averaged rainfall versus period and latitude for the two cases. As the aqua planet is longitudinally symmetric, this figure is produced by combining the statistics at each longitudinal point. The total rainfall is surprisingly white at all latitudes in both cases, although less so for the Kuo-Std case. The white spectra are in agreement with ISCCP cloud brightness spectra in the vicinity of the ITCZ (Hendon, personal communication 1990). With few exceptions the power in rainfall near the equator is larger in the MCA-Std than in the Kuo-Std case at all periods, especially equatorward of the rainfall maximum in Kuo-Std. In both cases prominent spectral peaks are associated with the ITCZ. In addition, the intraseasonal oscillation (also called the Madden-Julian and 30–60-day oscillation) can be identified with a period of about 25 days in both the Kuo-Std and MCA-Std runs. While the phenomenon is, however, more difficult to observe in the precipitation and momentum fields (not shown) in the Kuo-Std case, it is dominant in the MCA-Std case. The difference in the rainfall spectra between the two cases is remarkable and is simply one facet of the consequences of changing the convective scheme in a GCM. We anticipate from Fig. 3 that various wave types leave their imprint in these rainfall spectra and that the wave spectra differ considerably between the schemes. This is further discussed in section 5.

The zonal-mean velocities are shown for the two cases in Fig. 4. In the tropics, the low-level velocity profile shows little difference between the two cases. The evaporation due to the zonally averaged zonal component of the wind (as well as the net evaporation) is also very similar in each case (not shown). The subtropical jets in the MCA-Std case are stronger and are situated closer to the equator than in the Kuo-Std case. The tropospheric zonal velocities are significantly larger in the MCA-Std case between 38°S and 38°N than in the Kuo-Std run except in the lowest model levels

¹ In the Kuo-Std experiment the moist convective adjustment scheme is left on, so that subsequent to adjustment by the Kuo scheme any residual unstable layers are stabilized. The MCA scheme in this run, however, accounts for less than 10% of the total precipitation. The MCA scheme is not used in any of the other model integrations that have included the Kuo scheme.

TABLE 2. The experiments are identified in the left-hand column. The case is identified first by the type of convective scheme, either Kuo or moist convective adjustment, and then by the lower boundary sea surface temperature condition (see caption of Table 1). The second column indicates the location of ITCZ(s) for each model run. The zonal and time mean precipitation in the ITCZ(s) is found in column three, while the percentage of this precipitation that is convective (not large-scale precipitation) is indicated in column four. The location and speed of the subtropical jets are noted in the last two columns.

Case	ITCZ Location (°lat)		Precipitation (mm day ⁻¹)		Convective precipitation (%)		Jet location (°lat)		Jet speed (m s ⁻¹)		
	SH	NH	SH	NH	SH	NH	SH	NH	SH	NH	
Kuo-Flat	7	7	7.3	7.0	76	76	52	49	21	25	
Kuo-Feb1	10	7	10.8	8.0	71	77	40	40	46	45	
Kuo-Feb2	13	4	12.5	8.0	68	72	40	40	49	45	
Kuo-Oct	7	7	10.7	10.2	76	76	40	37	50	48	
MCA-Oct	7	7	7.4	8.0	62	62	40	36	51	51	
Kuo-Std	4.2-7	4.2-7	8.3	8.7	80	80	40	40	39	37	
MCA-Std		Eq		14.6		65		32	29	42	41
Kuo90-Std		Eq		11.5		15		37	32	36	44
Kuo-Peq		Eq		19.0		66		33	30	40	38
Kuo-Poeq		10°N		17.5		63		30	29	62	20
KuoNwv-Std		Eq		10.0		78		24	24	68	65

equatorward of 20°. We note that the jet axis in the Kuo-Std case is almost vertically oriented, whereas in the MCA-Std case the jet axis has a pronounced equatorward tilt leading to the equatorward position of the jets (in the lower troposphere the location of the jet axis is almost identical in each of the runs). We will further discuss the zonal-mean circulations in relation to the position of the ITCZ in section 6.

The convective heating for the two standard cases is shown in Fig. 5. Heating and vertical velocity are, to a good approximation, related to each other in the tropics by the static stability (Holton 1979). Hence,

the vertical velocity profile resembles the heating distribution in the vicinity of the ITCZs. The heating maximum due to convective processes in the MCA-Std case is found on the equator and is larger than the heating maxima in the Kuo-Std case. The Kuo-Std case has two vertical heating maxima in the ITCZ, located at about 6° latitude; one maximum just above the boundary layer and one near 500 mb. The lower heating maximum in the ITCZ of the Kuo-Std case is not echoed in the MCA-Std run. Consistent with numerous other studies, the upper-level heating maximum in the ITCZ of the Kuo-Std case is located slightly higher

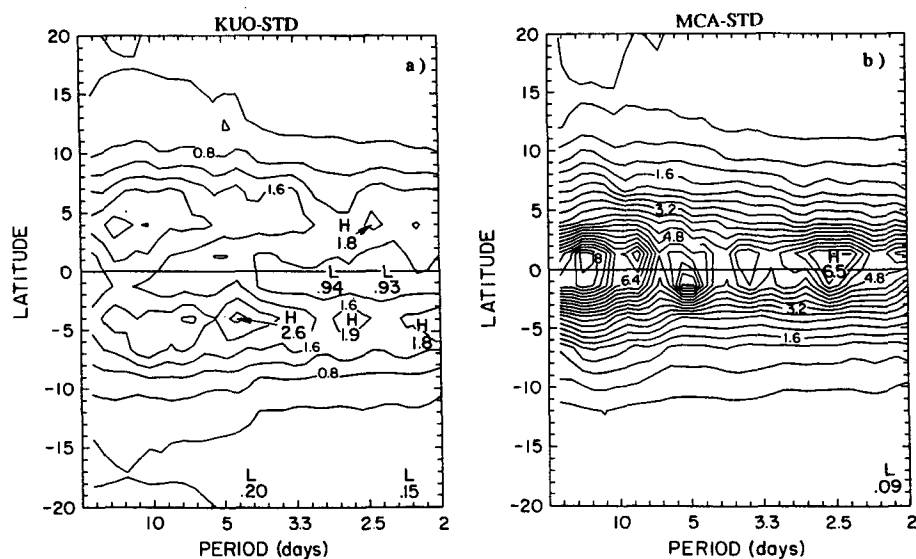


FIG. 3. The power spectrum for 12-hour averaged total precipitation in the (a) Kuo-Std and (b) MCA-Std case is plotted as a function of latitude and period. The spectra are based on 60-day time series. Contour interval is 0.4 mm² day⁻²/spectral estimate.

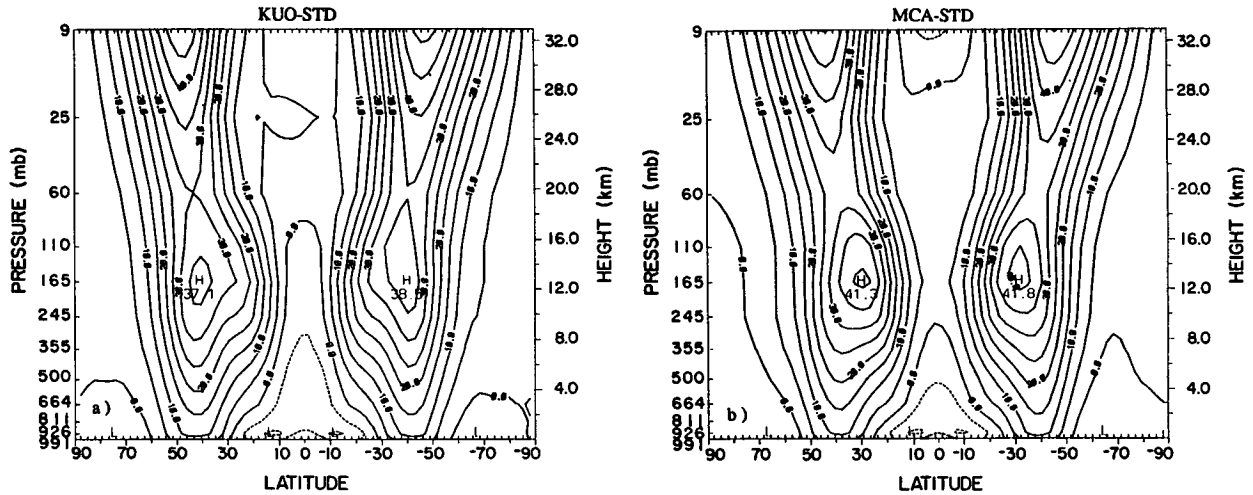


FIG. 4. A meridional cross section of the zonally averaged zonal velocity for the (a) Kuo-Std and (b) MCA-Std case. The time averages are over 60 days. The contour interval is 5 m s^{-1} .

than in the MCA-Std case. We also note that in the Kuo-Std case the heating is more evenly distributed in the vertical than in the MCA-Std case. Hence, both the time-averaged heating and transient convective heating are affected by the convective parameterization [cf. panels (a) and (b) in Figs. 3 and 5].

The mass streamfunction (Fig. 6) further emphasizes the differences in circulation between the Kuo-Std and the MCA-Std cases alluded to earlier. The rising branch of the Hadley circulation in the Kuo-Std case is latitudinally wider and the meridional circulation cells extend farther poleward than in the MCA-Std case. The meridional circulation in the MCA-Std case is almost 50% stronger than in the Kuo-Std case, with the upward motion confined to a narrow zone in the vicinity of the equator. This result is consistent with that of

Tiedtke et al. (1984), who finds the ECMWF (T42) forecast model with the Kuo scheme has a much weaker zonally averaged Hadley circulation compared to that in the model with the MCA scheme (see also Hart et al. 1990). These results are also consistent with Schneider (1977), who argues that a concentrated heat source will produce a Hadley circulation stronger than that produced from a diffuse heat source with the same integrated heating.

Moist static energy (H) for the Kuo-Std and MCA-Std cases is shown in Fig. 7. Here H is defined as the sum of the dry static energy, S , and the potential energy due to water vapor mixing ratio, Lq :

$$H = S + Lq = c_p T + gz + Lq, \quad (1)$$

where q is the water vapor mixing ratio, T is the tem-

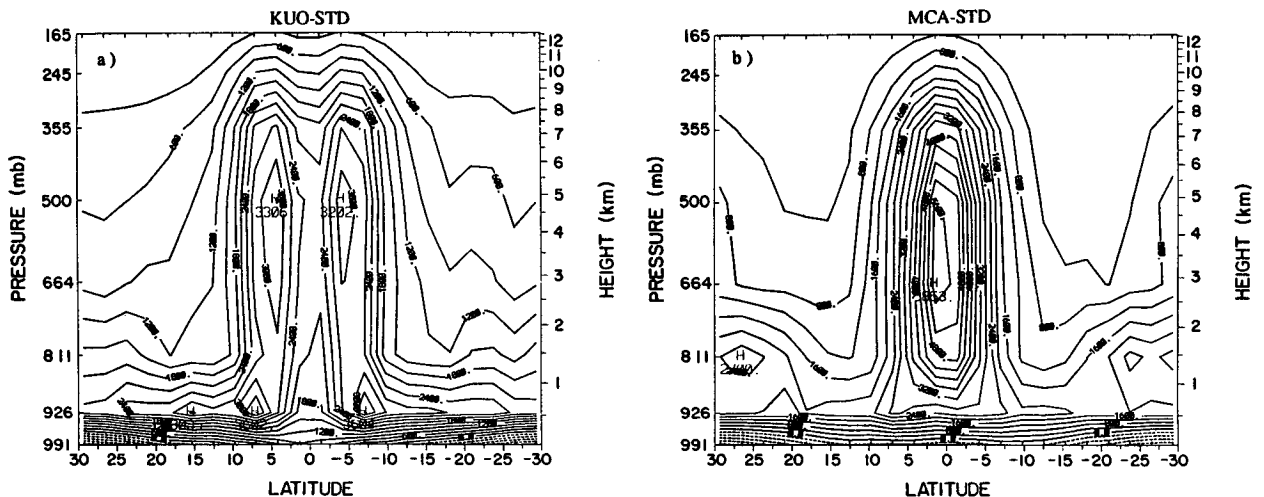


FIG. 5. A meridional cross section of the zonally averaged latent heating for the (a) Kuo-Std and (b) MCA-Std case. The time average is over 60 days. The contour interval is 300 $\text{J kg}^{-1}/\text{day}$ in (a); 400 $\text{J kg}^{-1}/\text{day}$ in (b).

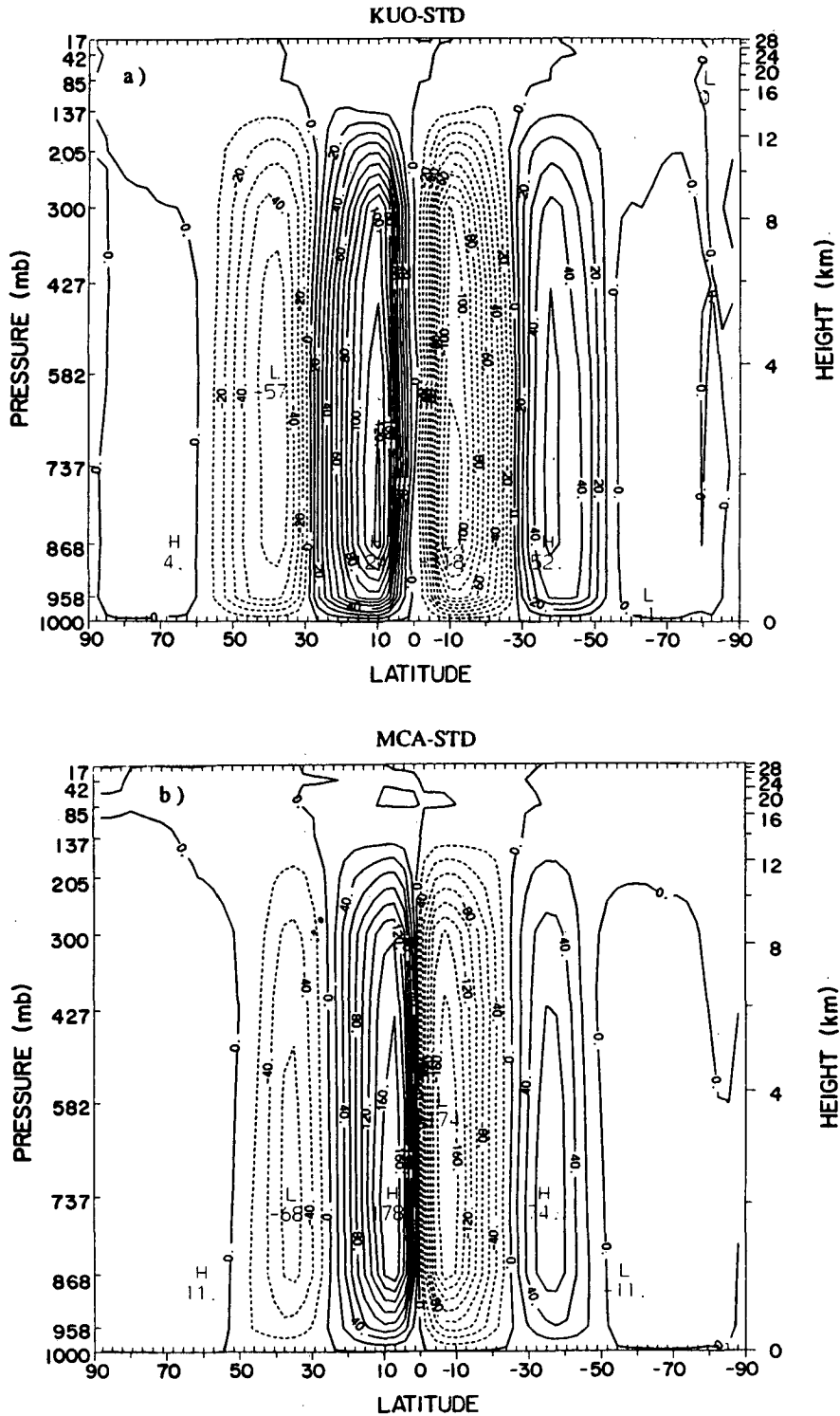


FIG. 6. A meridional cross section of the zonally averaged meridional mass streamfunction for the (a) Kuo-Std and (b) MCA-Std case. The time average is over 60 days. The contour interval is $1 \times 10^{10} \text{ kg/m s}^{-1}$ in (a); $2 \times 10^{10} \text{ kg/m s}^{-1}$ in (b). Labels are scaled by $10^{-10} \text{ kg/m s}^{-1}$.

perature, c_p the specific heat of air, L the latent heat of condensation, z the geometric height, and g the acceleration due to gravity. The distribution of the zonal,

time-mean moist static energy is similar in the two cases. In each case the vertical gradient of moist static energy is small above 811 mb and over the region of

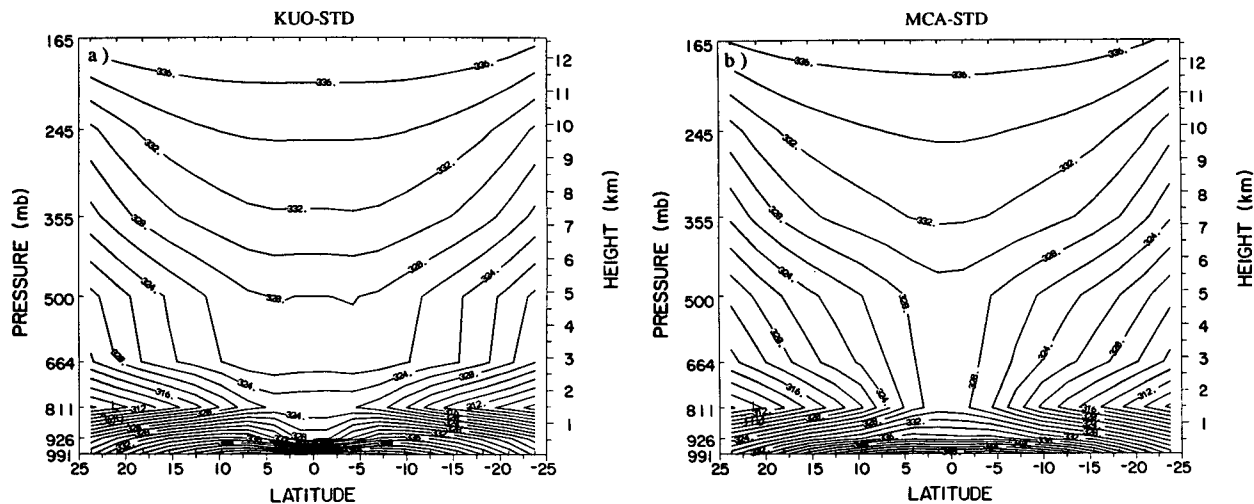


FIG. 7. A meridional cross section of the zonally averaged moist static energy H for the (a) Kuo-Std and (b) MCA-Std case. The time averages are over 60 days. Labels are scaled by 0.001 and the contour interval is 2000 J kg^{-1} .

active convection. Also, throughout the subtropics and poleward of 5° latitude a moist boundary layer, marked by high values of moist static energy, is capped by a thin layer (from 811 to 664 mb) of dry air with relatively low moist static energy. Independent of whether the MCA or Kuo convective scheme is used, in the time average the modeled tropics are conditionally unstable below 500 mb and, within the region of the model ITCZs, the atmosphere is in approximate radiative-convective equilibrium (not shown).

4. The influence of the large-scale environment on convection

The distribution of the zonal, time-mean moist static energy (Fig. 7) in the MCA-Std case is qualitatively similar to that in the Kuo-Std case. The time-mean circulation (e.g., the number and location of the ITCZs) and tropical transients (Fig. 3; see also section 5), however, are very different in the two cases, implying that the two convective schemes adjust the atmosphere in different ways. This is to be expected since the Kuo and MCA convective adjustment parameterizations have different criteria to diagnose the occurrence of convection, and use different criteria to determine the vertical extent of convection and the subsequent redistribution of energy and mass (see section 2b).

In this section we document the disparate manner in which the Kuo and moist convective adjustment schemes interact with the large-scale environment. Specifically, it will be shown that the Kuo scheme effectively and efficiently couples the boundary-layer circulation to the convective forcing of a *deep* tropospheric column of air (section 4a). By contrast, the coupling of the boundary-layer circulation to the free atmosphere circulation in the model with the MCA scheme depends on a subtle interaction between

boundary layer and free atmospheric (vertical) motions (section 4b); this scheme rarely adjusts more than three contiguous layers. The differences in the convective schemes cause the mean maximum convection (the ITCZ) to be located at different latitudes (shown in section 4c) and crucially affect the nature of the tropical transients and the structure of the time-mean circulation (see also sections 5 and 6).

To identify the large-scale conditions in which convection occurs in the CCM we examine the vertical profiles of relative humidity, moist static energy, horizontal moisture convergence, and vertical velocity immediately prior to when the atmosphere is convectively adjusted in the Kuo-Std and MCA-Std model runs. We categorize the column of air over each horizontal grid location as either a convectively precipitating column (CPC) or a nonconvectively precipitating column (NCPC). The NCPCs are, by definition, not directly affected by the convective parameterization. However, we examine the CPCs *immediately* prior to the convective adjustment, whereafter the temperature and moisture characteristics of these columns of air are subsequently changed. All diagrams show the composite of the CPCs and NCPCs for grid points between 4.2°N and 4.2°S for two model time steps. In both the Kuo-Std and MCA-Std runs this range of latitudes includes the ITCZ. In the Kuo case 26% of the points are in CPCs, while in MCA 14% of the points are convectively precipitating.

a. The Kuo-Std experiment

Figure 8 shows selected composite vertical profiles for CPCs and NCPCs for the Kuo-Std and MCA-Std model runs. With both parameterizations convection tends to occur in columns when there is large-scale upward vertical velocity throughout the troposphere (Figs. 8a and 8e) and horizontal moisture convergence

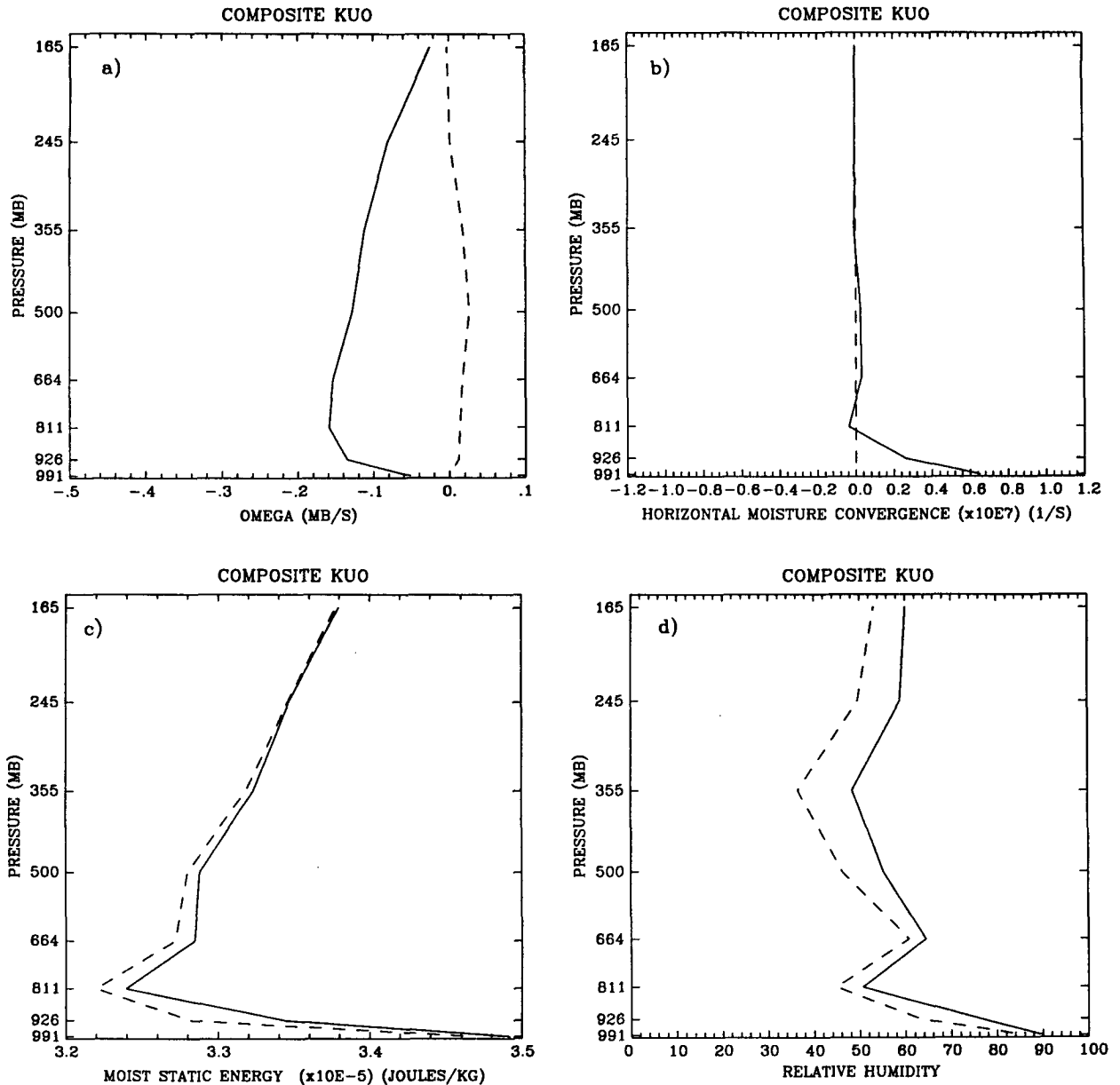


FIG. 8. Composite vertical profiles for (a–d) the Kuo-Std case and (e–h) the MCA-Std case of CPCs (solid line) and NCPCs (dashed line) for vertical velocity ω (mb s^{-1}) (a, e); horizontal moisture convergence (s^{-1}) scaled by 1×10^7 (b, f); moist static energy scaled by 1×10^{-5} (c, g); and relative humidity (%) (d, h). All points located between 4.2°N and 4.2°S for two model time steps are included in the composite.

(Figs. 8b and 8f). Columns that do not convect exhibit weak subsidence and feature very little moisture convergence. In the model with the Kuo parameterization, the convecting and nonconvecting columns have very similar profiles of relative humidity and moist static energy (Figs. 8c and 8d). We note that the boundary layer is much more pronounced in the Kuo-Std run than in the MCA-Std run. As a result, the air above the boundary layer is much drier in the Kuo-Std case: at 811 mb in the Kuo-Std case, both the moist static energy and equivalent potential temperature (θ_e , not

shown) in convecting columns are *less* than that in the nonconvecting columns using the MCA scheme.

From Figs. 8a–d it is clear that the only dramatic difference between CPCs and NCPCs using the Kuo scheme is in the profile of vertical velocity, and horizontal moisture convergence below 811 mb in the boundary layer. A scatterplot of the vertical velocity and horizontal moisture convergence at the 991-mb level immediately prior to convection is shown in Fig. 9a for the Kuo-Std case. The open circles represent the characteristics of the CPCs immediately prior to when

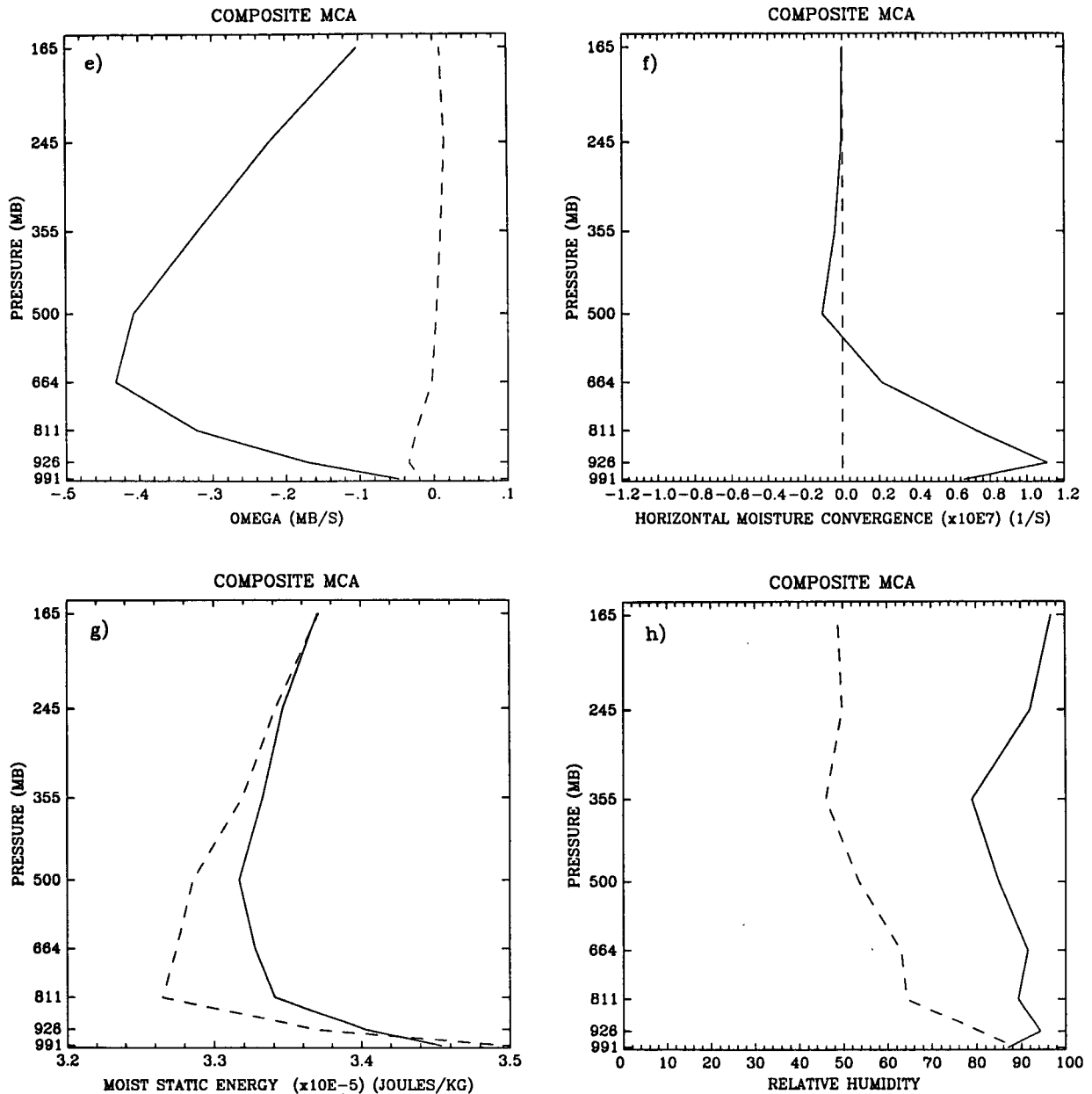


FIG. 8. (Continued)

the column is convectively adjusted by the Kuo scheme; the characteristics of the various NCPs are represented by the dots. The CPCs shown are not actually convecting at 991 mb: typically the convective cloud is initiated at 926 mb and extends throughout the model troposphere. It is clear that there is no convection anywhere in a column that has downward motion at 991 mb. Columns with modest upward vertical velocities at 991 mb and especially those with positive horizontal moisture convergence are likely to convect. The clear separation between convectively precipitating and nonprecipitating points indicates a very high correlation between boundary-layer moisture convergence

and convection with the Kuo scheme: approximately 70% of the convective columns have positive moisture convergence at 991 mb, and there are very few columns with both positive horizontal moisture convergence and upward vertical velocities at 991 mb that do not convect. Hence, in the deep tropics convection is rarely limited by the additional criteria for the Kuo scheme to operate (see section 2b). Figure 9a, along with the composite profiles (Fig. 8), suggests that when horizontal moisture convergence occurs within the boundary layer using the Kuo scheme, irrespective of the vertical profile of moisture (or θ_e ; not shown) above the boundary layer, convection will occur. The rather sharp

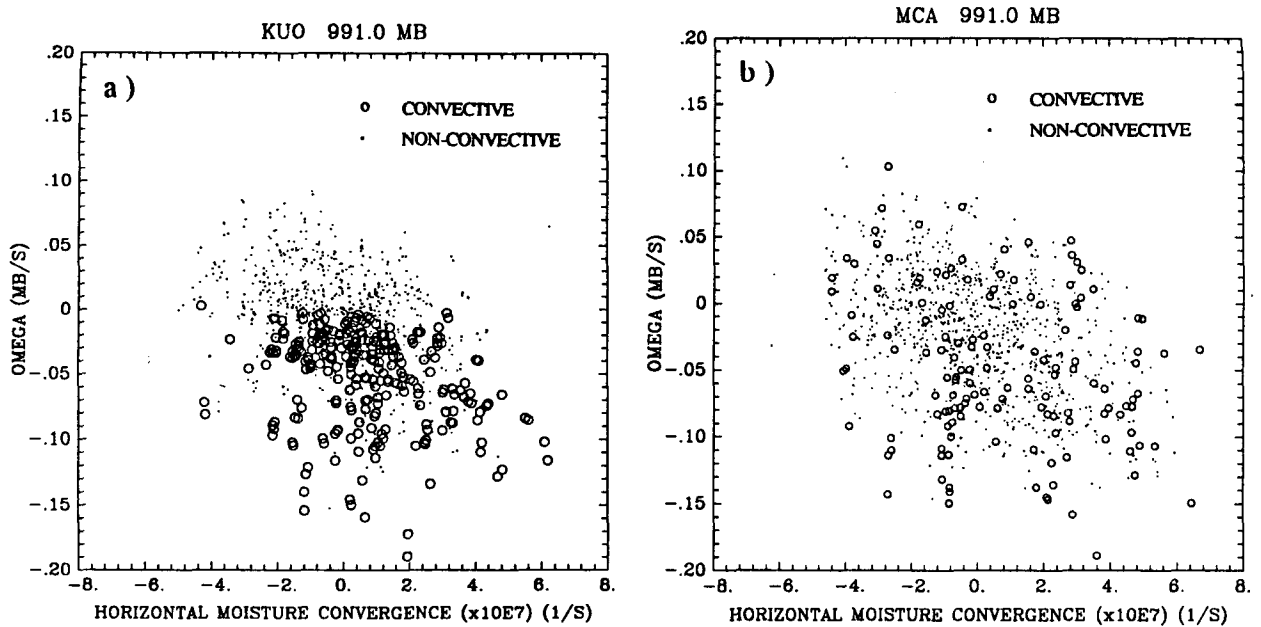


FIG. 9. (a) A scatterplot of the convective characteristics of a column of air as a function of vertical velocity ω (mb s^{-1}) and horizontal moisture convergence $-\nabla \cdot (q\mathbf{v})$ (s^{-1}) at 991 mb for the Kuo-Std case. A circle (dot) indicates air at 991 mb is (is not) embedded in a column of air that is about to undergo convection *somewhere* in the column. The same points plotted are used for the composites in Fig. 8. (b) As in (a), but for the MCA-Std case.

inversion of moist static energy at the top of the boundary layer does not need to be eroded, nor does the moisture convergence have to be particularly strong, for convection to occur.

b. The MCA-Std experiment

The criterion for convective adjustment in the MCA scheme is that air must be saturated at *two* consecutive levels and have an unstable lapse rate. As clouds cannot form at the lowest model level, the first contiguous layers that can convect are 926 and 811 mb. The air at 811 mb is, however, on average very dry (Figs. 8g and 8h) because the upward transport of moisture from within the boundary layer is generally hindered by the drying due to weak subsidence aloft. Hence, while the atmosphere is conditionally unstable to 500 mb in both the convecting and nonconvecting composite (not shown), it requires an extraordinary amount of lift (~ 1500 m) to destabilize the air at and above the top of the boundary layer in the nonconvecting columns.

Nonconvecting columns in the model using the MCA scheme have similar signatures in relative humidity and moist static energy to both NCPCs and CPCs in the model with the Kuo scheme: similarly, throughout each of the NCPCs moisture convergence is weak (Fig. 8f) and there is subsidence above 664 mb (Fig. 8e). However, while there is weak subsidence above 644 mb in the composite nonconvecting column in the MCA-Std case, it is important to note that in

the vicinity of the time-mean ITCZ NCPCs have weak upward vertical velocity within the boundary layer below 811 mb (cf. Fig. 8e for Kuo-Std).

In the model with the MCA scheme, columns that are about to convect (CPCs) have a remarkably different vertical distribution of moist static energy (Fig. 8g), relative humidity (Fig. 8h), and equivalent potential temperature (not shown) from those that will not subsequently convect (NCPCs). Convection is diagnosed to occur in columns that are “preconditioned” to have increased moist static energy (and θ_e) between 500 and 811 mb (Fig. 8g) when compared to the nonconvecting (“environmental”) columns. This increase in moist static energy is largely due to an increase in moisture, and is accomplished primarily through vertical advection of moisture from below (Figs. 8e,f,h). Columns that are about to convect in the MCA-Std case display a much deeper layer of horizontal moisture convergence (to ≈ 550 mb) than in the nonconvecting composite. Note that, unlike the Kuo-Std case, the in situ near-surface vertical velocity together with the horizontal water vapor convergence do not distinguish columns that will convect from those that do not in the MCA-Std case (cf. Figs. 9a and 9b). Hence, convection in the MCA scheme is not as closely tied to shallow convergence within the boundary layer as it is using the Kuo convective parameterization.

The easiest way to moisten air at 811 mb is to advect moisture from below. Figure 10 shows that those columns with high relative humidity at 811 mb also tend to have strongly upward motion, consistent with the

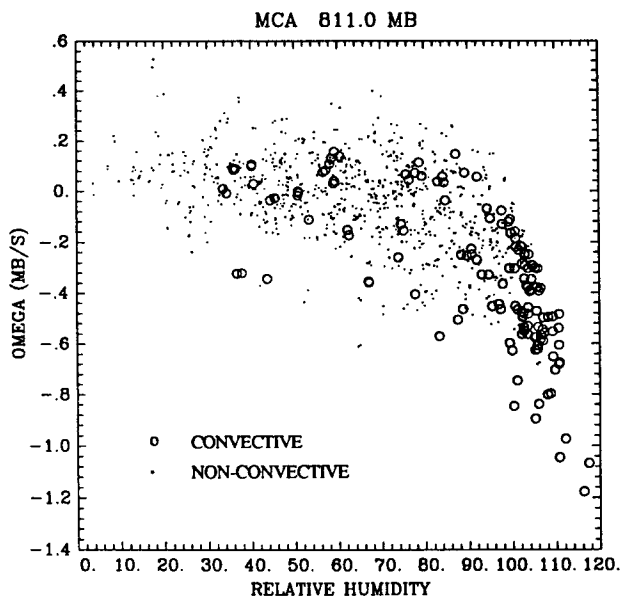


FIG. 10. As in Fig. 9 but for vertical velocity ω and relative humidity for the MCA-Std run at 811 mb. Relative humidity is in percent, ω is in mb s^{-1} .

conclusion that a robust upward motion is necessary to moisten the 811-mb layer sufficiently for convection to occur. It is evident from this figure that when the vertical velocity is strongly upward and the relative humidity is very high, moist convective adjustment is likely to occur somewhere in the column: a large upward vertical velocity will quickly saturate and destabilize the column. Otherwise, convection is unlikely.

The difference between H at 991 mb and H at 811 mb versus the relative humidity at 926 mb discriminates CPCs from NPCCs in the MCA-Std case (Fig. 11). As the moist static energy at 991 mb is strongly tied to the SST, the difference between H at 811 mb and that at 991 mb is dominated by changes in H (via changes in moisture) at 811 mb, the top of the boundary layer. Air at 926 mb with high relative humidity and with small differences in H between the boundary layer and that at 811 mb indicates the large moist static energy in the boundary layer has been transported upwards (see also Fig. 8g) by advection (moisture convergence), allowing air above the boundary layer to become unstable and convect.

Contrary to the Kuo scheme, which usually adjusts the entire troposphere when implemented, the MCA scheme rarely adjusts more than three vertical levels at a time (not shown). For example, Fig. 10 indicates that although saturation at 811 mb is often associated with convection somewhere within that particular column, only 50% of the columns are actually convecting at 811 mb (the rest are not saturated at this level). Hence, unlike the Kuo scheme, the MCA scheme links the convective heating above boundary layer to the remaining troposphere in an indirect manner.

c. Summary of convection—Large-scale interactions

We can now understand why the ITCZ is found over the warmest water in both CCM integrations using the MCA scheme for convection (MCA-Std and MCA-Oct; Table 2). For convection to occur in the model with the MCA scheme, a moistening (preconditioning) of the dry air immediately above the boundary layer is necessary. This is largely accomplished by vigorous vertical advection of moisture. The Kuo scheme does not require such extensive preconditioning for convection to occur (cf. the NPCC and CPC profiles of moisture for the Kuo-Std and MCA-Std cases; Figs. 8d and 8h).

It is clear from the preceding discussion (section 4b) that with the MCA parameterization, the preferred location for convection will be where the mean near-surface boundary-layer circulation features upward-moving air of high moist static energy. For a boundary layer sufficiently decoupled from the upper atmosphere (unlike the boundary layer in the Kuo-Std case), the maximum low-level vertical velocity (convergence) is over the warmest water because, in absence of other processes, SST gradients induce hydrostatic pressure gradients that force a boundary-layer circulation with a maximum upward vertical velocity over the region where the SST is maximum (Schneider 1977; Lindzen and Nigam 1987; Neelin 1989). This is consistent with Fig. 8e, which shows that in the vicinity of the maximum SST (equator) the composite vertical velocity is upward in the MCA-Std boundary layer for both CPCs and NPCCs. It is in this sense that the convection (hence, the ITCZ location) is intimately related to the SST distribution when the MCA scheme is used in the

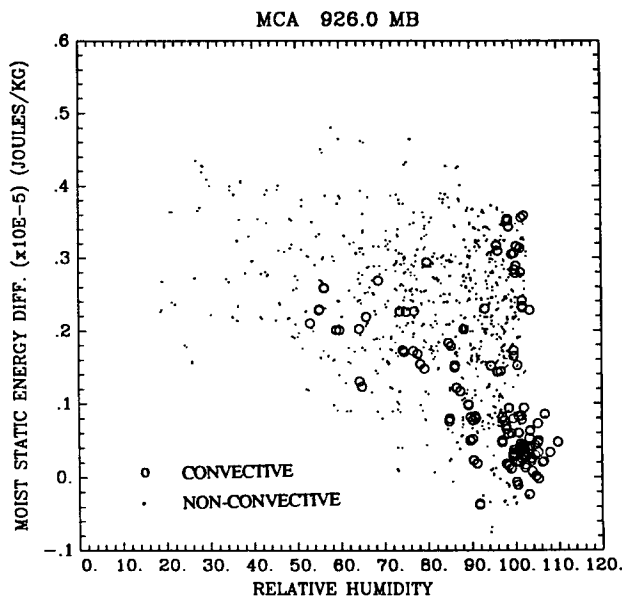


FIG. 11. As in Fig. 9 but for the difference between H at 991 mb and H at 811 mb versus the relative humidity at 926 mb for the MCA-Std run. H is in J kg^{-1} , relative humidity is in percent.

CCM. Finally, when convection occurs it usually affects a shallow layer of air (two or three contiguous layers). Hence, the diabatic heating associated with the adjustment of middle- and upper-tropospheric air is not explicitly connected to low-level convection.

The sufficient criteria for convective adjustment in the same model but with the Kuo scheme are weak convergence and upward motion *within* the boundary layer. Convection occurs even in the presence of dry air immediately above the boundary layer and is not preceded by changes in the buoyancy (through moistening) of the dry air at this level. In almost all instances, convective adjustment by the Kuo scheme extends throughout the troposphere. As will be shown in the next section, the extreme sensitivity of the Kuo scheme to weak convergence in the boundary layer leads to enhanced convection off the equator, away from the warmest water, via efficient boundary-layer organization by transient motions.

5. The effect of the zonal asymmetric motions

The analysis of section 4 indicates that for both convective schemes the vertical velocity is important in determining where and when convection will occur. Employing the MCA scheme in the GCM, the upward motion required for convection to occur is focused over the warmest water via surface gradients in diabatic heating. The latter create large-scale hydrostatic pressure gradients that cause the boundary-layer flow to be convergent over the warmest water. In contrast, the upward motion required for convection in the model with the Kuo scheme is weak, and the associated moisture convergence is limited to a very shallow surface layer. This convergence could be initiated by equatorial wave transients or Ekman pumping induced by wave transients.

In this section we test the hypothesis that the interaction between the wave transients and the parameterized convection may affect the ITCZ and hence the zonal time-mean circulation. First we will discuss an axisymmetric simulation, which allows no zonally propagating disturbances, to demonstrate the importance of wave transients. We will then focus on the highly energetic transients in the 3–4-day band in a subset of four model runs to examine the relationship between the location of the ITCZ, the zonally asymmetric transients, and the parameterization of moist convection. We find in some of the experiments much of this energy can be explained by mixed Rossby–gravity waves. We conclude that the equatorial wave spectrum and the location of the ITCZ are indeed mutually interdependent. One of the primary reasons the general circulation model realizes very different time-mean climates using the Kuo and MCA schemes (the Kuo-Std and MCA-Std cases) is the disparate manner in which the parameterized convection interacts with the equatorially trapped transient waves when using the two schemes.

To eliminate all zonally asymmetric wave transients we integrate the CCM with the Kuo convective adjustment scheme in an axisymmetric (2D) configuration (the Kuo Nwv-Std case) using the zonally averaged ending condition for the Kuo-Std integration for initial conditions. This model configuration does not permit zonally propagating disturbances. Thus, the only significant model change from the Kuo-Std case is the reduction in the degrees of spatial freedom. (Diffusion in the “stratosphere” is enhanced in the Kuo Nwv-Std case model to stabilize the numerics.) After a few days of model integrations, the double-ITCZ structure in the initial conditions erodes in the Kuo Nwv-Std run. In the time-mean circulation a well-defined single ITCZ is found on the equator, indicated by the distribution of precipitation displayed in Fig. 2b. We conclude that the zonally asymmetric transients are clearly an important element in producing the steady-state solution in the Kuo-Std case, moving the ITCZ off the equator and modifying the attendant large-scale mean tropical circulation. Transients lead to increased convection off the equator because they provide an efficient means of organizing off-equatorial vertical motion, particularly in the boundary layer via friction (see section 4b).

The ITCZ in the axially symmetric CCM (with the Kuo scheme) is found over the warmest water, located on the equator in this instance. This is consistent with the results of the other axially symmetric simulations (Schneider 1977; Schneider and Lindzen 1977; Pike 1971; Goswami et al. 1984) and the MCA-Std case, but contrary to the results of the fully three-dimensional Kuo-Std simulation. The axisymmetric Kuo integration (Kuo Nwv-Std) does allow the physics postulated by Charney (1971) for maintaining off-equatorial ITCZs: the competition between the efficiency of Ekman pumping and the amount of moist static energy. Nonetheless, the circulation in the Kuo Nwv-Std case, characterized by one ITCZ on the equator, is contrary to Charney’s hypothesis. On the other hand, the importance of the zonally asymmetric transients in the Kuo-Std simulation, made apparent by the Kuo Nwv-Std experiment, is consistent with the Holton et al. (1971) hypothesis for maintaining the off-equatorial ITCZs but it does not prove that the postulated mechanism is indeed occurring.

Holton et al. specifically suggest 4–5-day waves may be important in organizing surface moisture convergence and, hence, convection off the equator. These waves were implicated, in part, because they are a ubiquitous feature of the tropical troposphere (Wallace and Chang 1969; Reed and Recker 1971; Nitta et al. 1985). Liebmann and Hendon (1990) have identified the 4–5-day signal in the central Pacific, and possibly in the eastern Pacific in boreal spring, as westward-propagating mixed Rossby–gravity waves. In the integrations we have performed the vigorous wave activity associated with the observed 4–5-day band appears to be shifted towards shorter periods, to about 3–4 days. This shift is consistent with the frequency shift in the

intraseasonal oscillation found in most GCMs (e.g., Hayashi and Sumi 1986; Lau et al. 1988), including the CCM. We will focus on this highly energetic 3–4-day band and the mixed Rossby–gravity waves in a subset of model runs to examine the relationship between the location of the ITCZ and the zonally asymmetric transients using both Kuo and moist convective adjustment schemes. It is important, however, to emphasize that the difference between the wave spectrum in the two standard model runs is not limited to the mixed Rossby–gravity waves in the synoptic band (e.g., see Fig. 3).

Mixed Rossby–gravity waves are antisymmetric about the equator in zonal velocity and geopotential with maximum amplitude between 7° and 10° latitude (Matsuno 1966). The wave convergence field is also antisymmetric about the equator and, above the boundary layer, is a maximum at the latitude of the minimum in geopotential (see Holton et al. 1971). Mixed Rossby–gravity waves feature a meridional wind that is strongest on, and symmetric about, the equator. It is the only tropical wave with strong meridional wind on the equator. For this reason we perform a spectral analysis on the symmetric meridional wind, v_{eq} , defined as the mean of the modeled meridional wind fields at 7° N and 7° S. We compare cases for each convection scheme that are characterized by a single ITCZ on the equator and by two off-equatorial ITCZs: the Kuo-Std and the MCA-Oct model runs, each with a double ITCZ structure, and the Kuo-Peq and the MCA-Std model runs, each with a single ITCZ on the equator.

Each of the four cases enumerated above has a spectral peak in the equatorial meridional wind (v) between about three and four days, significant at the 99% confidence level. In all cases, except for Kuo-Peq, the spectral peaks in v are centered on the equator and decay within 10° of the equator (not shown). In the Kuo-Peq case the power in v maximizes near $\pm 5^\circ$ latitude, although power along the equator is also maximum at this period. The spectral peak in symmetric meridional velocity v_{eq} is found between 800 and 900 mb in all four cases, consistent with the observed mixed Rossby–gravity waves in the lower troposphere (Wallace and Chang 1969; Liebmann and Hendon 1990). The wavenumber–period spectra for the symmetric meridional wind at 811 mb and for westward-moving disturbances are displayed for the four cases in Fig. 12. As the model is zonally symmetric, the statistics for all 128 longitude points are combined. In all cases except for the MCA-Std case there are distinct spectral peaks in these plots between about three and four days. The maximum power in this frequency band decreases from Kuo-Std (max $\sim 0.04 \text{ m}^2 \text{ s}^{-2}$) to MCA-Oct (max $\sim 0.025 \text{ m}^2 \text{ s}^{-2}$) to Kuo-Peq (max $\sim 0.01 \text{ m}^2 \text{ s}^{-2}$) to MCA-Std, which has the least power (max $\sim 0.009 \text{ m}^2 \text{ s}^{-2}$). In each case the power in v_{eq} is a maximum at wavenumber 4 in this period interval. A second maxima occurs between wavenumbers 8 and 11, depending on the case.

A more complete analysis using the lag-correlation method of Fraedrich and Lutz (1986) is performed on v_{eq} for the MCA-Std and Kuo-Std cases. In the Kuo-Std case the analyzed frequency, phase, and group velocity in the 3–4-day band at wavenumber 8 are consistent with associated dispersion characteristics for the mixed Rossby–gravity mode: the dispersion curve is plotted in Fig. 12a. In the MCA-Std case the analyzed phase and group velocity associated with the maximum power in the wavenumber–period plot are not consistent with the mixed Rossby–gravity dispersion relationship. Subsequent regression analyses (to be published) show that well-defined mixed Rossby–gravity waves do exist for the Kuo-Std and the MCA-Oct cases, with two off-equatorial ITCZ, but not for the Kuo-Peq and MCA-Std cases, which display a single ITCZ on the equator.

We have computed lag correlations of the daily values of the 811-mb equatorial meridional wind with the zonal velocity at all points within 20° of the equator and at the same longitude for each of the four model experiments (" $v_{eq} \times u$ "; Fig. 13). The $v_{eq} \times u$ statistics are computed in the same way as the power spectra, except that the time series is daily for 64 days. The period of the maximum power in v_{eq} is indicated by an \times on the equator in Fig. 13; it is essentially the power shown in Fig. 12 integrated over wavenumber. The MCA cases show a slight tendency for $v_{eq} \times u$ to maximize near the frequency where the power in v_{eq} is maximum. In both Kuo cases, however, there are well-defined peaks at periods near 3.5 days (coinciding with period of the peaks in maximum power of v_{eq}) in $v_{eq} \times u$, maximizing between 5° and 9° off the equator. Within these regions of high correlation the southerly meridional wind leads (lags) the westerly zonal wind north (south) of the equator by approximately one-quarter cycle (Figs. 13a,c). The 3–4-day spectral peaks in meridional wind, and spatial distribution of these maxima in the model, are similar to the observed spectra (Wallace and Chang 1969; Liebmann and Hendon 1990; Hendon and Liebmann 1991), albeit at slightly higher frequency. The structure in the $v_{eq} \times u$ lag correlations is consistent with the correlations in the observed data and the theoretical mixed Rossby–gravity wave structure (Matsuno 1966).

It is interesting that when the Kuo scheme is used, the correlation between v_{eq} and u is in fact stronger when the precipitation is concentrated on the equator, suggesting the precipitation in the cases with the off-equatorial ITCZ degrades the wavelike relationship between v_{eq} and u . We note, however, that in the model runs utilizing the Kuo convective parameterization the symmetrical component of v_{eq} is almost four times as strong when the precipitation is off the equator (Kuo-Std) than when it is centered over the equator (Kuo-Peq).

Figure 14 shows the cross correlation between v_{eq} and the accumulated 12-hour averaged precipitation along a longitude line, extending 20° from the equator

Figure 14 shows the cross correlation between v_{eq} and the accumulated 12-hour averaged precipitation along a longitude line, extending 20° from the equator in the four cases. In each case (except Kuo-Peq) there is a region of high coherence around 5° to 7° latitude in the 3–5-day band that is roughly symmetric about the equator: the correlation squared is significant above the 99% level in each case. In the MCA-Std case the correlations between v_{eq} and precipitation are very broadbanded, consistent with the white rainfall spectrum of Fig. 3b. The two cases with off-equatorial ITCZ (Kuo-Std and MCA-Oct) show some indication of a localized correlation maxima near the frequency where

the power in the meridional wind maximizes on the equator and the maximum correlation is approximately collocated with the time-mean ITCZ. In addition, for these two cases the structure highlighted in the two cross-correlation plots [panels (a) and (d) of Fig. 13 and 14] is consistent in phase and location with the “moist” mixed Rossby–gravity wave described by Holton et al. (1971), Chang (1973), Liebmann and Hendon (1990), and Hendon and Liebmann (1991). To some extent a modest correlation between precipitation and v_{eq} is expected because precipitation is inherently noisy and nonnormally distributed. An analysis of the wavenumber frequency spectra associated

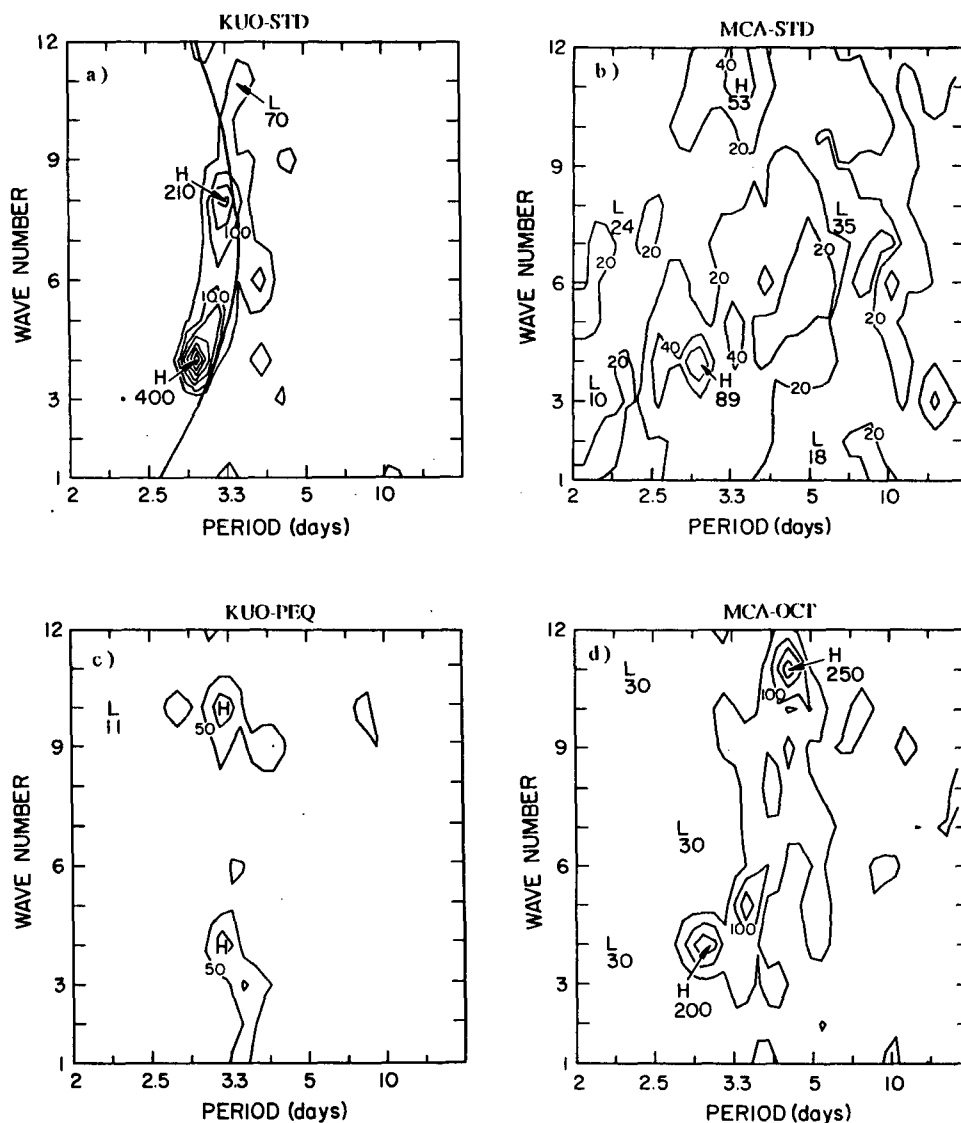


FIG. 12. The 811-mb wavenumber versus frequency spectra scaled by 1×10^4 for the symmetric meridional wind v_{eq} and westward-moving disturbances: (a) Kuo-Std, (b) MCA-Std, (c) Kuo-Peq, and (d) MCA-Oct. The theoretical mixed Rossby–gravity wave dispersion line is drawn for the Kuo-Std case (a). The spectra are based on daily data for a 75-day time series. Period is plotted on the abscissa. Units are $(\text{m s}^{-1})^2/\text{spectral estimate}$. The contour interval is 0.005 except for panel (b) which is 0.002.

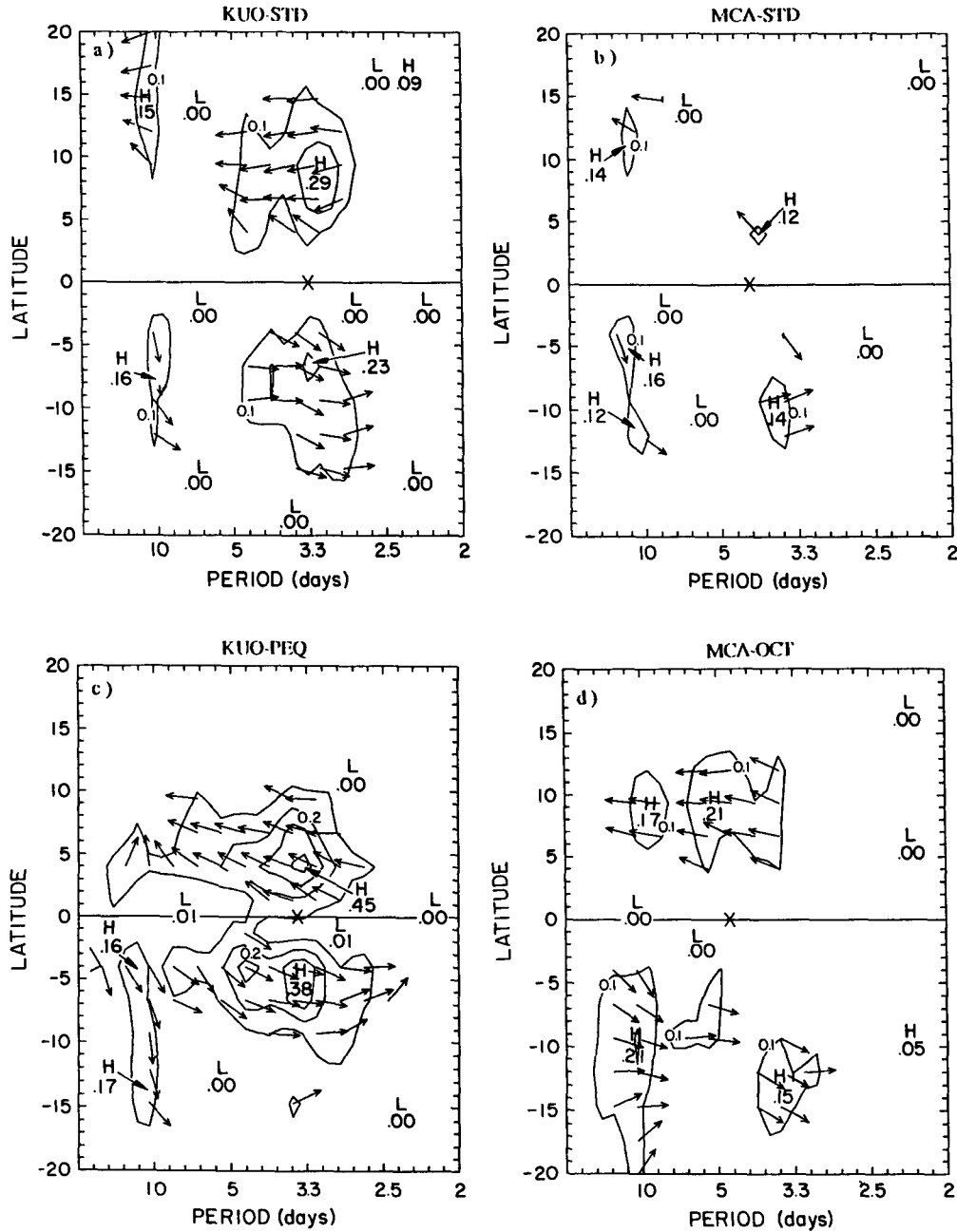


FIG. 13. The cross correlation of 811-mb symmetric meridional wind v_{eq} with the zonal velocity at all points within 20° of the equator for four of the model experiments: (a) Kuo-Std, (b) MCA-Std, (c) Kuo-Peq, and (d) MCA-Oct. The coherency squared is contoured (contour interval 0.1). The vector represents the amplitude and phase lag at maximum coherency: a left-pointing vector indicates northward v_{eq} leads eastward u by one-quarter cycle; an upward-pointing vector denotes no phase lag. The maximum power in v_{eq} is noted by an \times on the frequency axis. The time series are daily values for 64 model days. The statistics for all 128 longitude points are combined. Assuming only eight of these are independent yields 32 degrees of freedom and a coherency squared of 0.14, significant at the 99% level.

with *antisymmetric* precipitation (not shown), however, indicates no strong peaks within the 3–4-day band in the four cases examined here. Hence, it does not appear the wave transients in the 3–4-day band alone account for a significant percentage of the precipitation

in these runs. We conclude the collapse of the two ITCZ in the Kuo-Std case to one ITCZ in the Kuo Nwv-Std case appears to be due to the reduction of the collective transient mechanisms (i.e., the elimination of zonally propagating Rossby waves, mixed Rossby-gravity

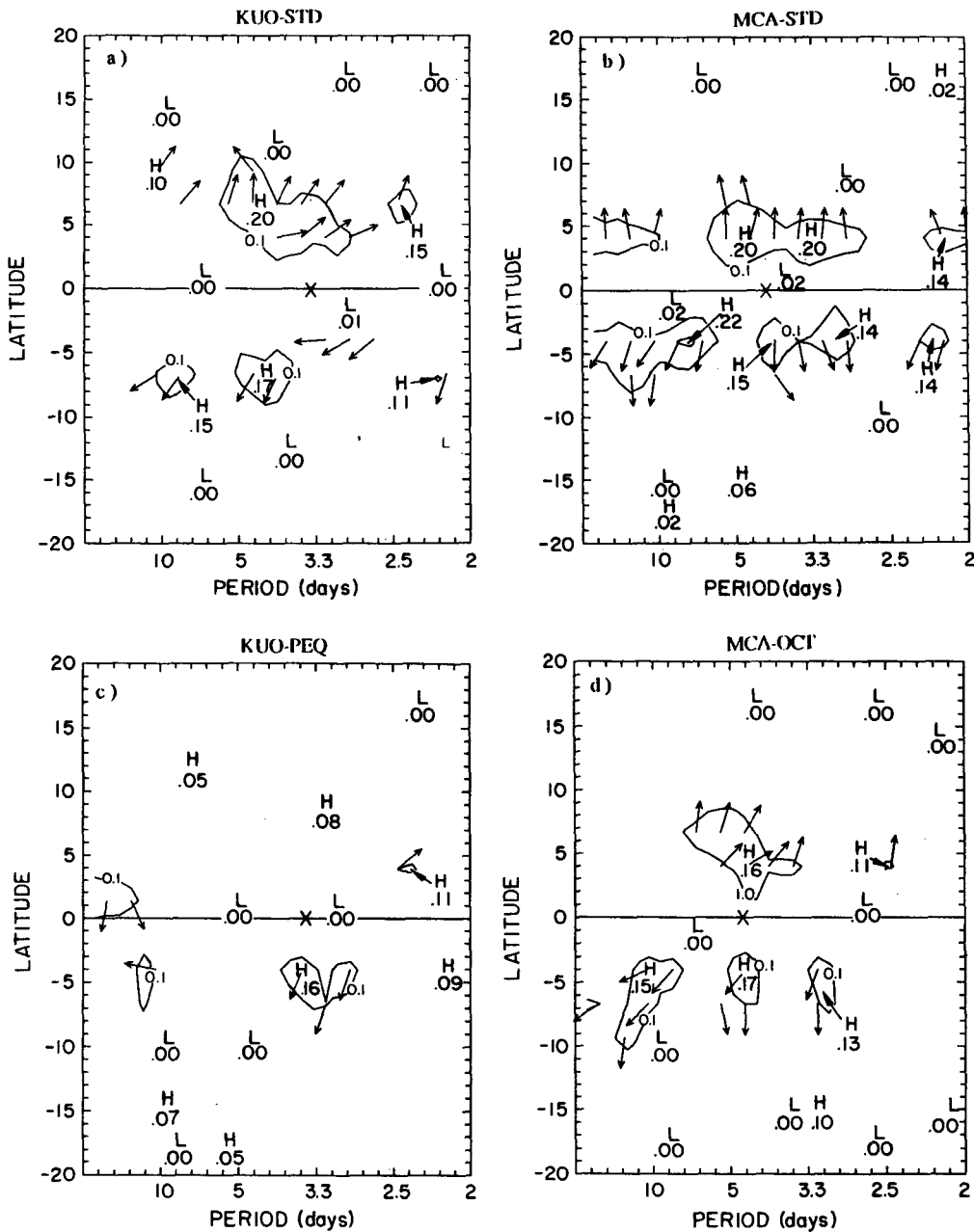


FIG. 14. As in Fig. 13 but for 811-mb v_{eq} with the precipitation at all points within 20° of the equator. The contour interval is 0.1.

waves, and other zonally asymmetric transients) in the two-dimensional geometry that can efficiently organize the boundary-layer flow off the equator.

Together the spectral analysis, cross correlation, and dispersion analysis of the synoptic band (as well as Fig. 3) demonstrate that the convective scheme has a significant impact on both location of the convection and the equatorial wave spectrum. The three-dimensional structure and the dispersion characteristics of the synoptic energy (frequency and wavenumber, phase and group velocities) in the Kuo-Std case are consistent

with a mixed Rossby-gravity wave, described by Matsuno (1966). A synoptic mixed Rossby-gravity wave does not stand out in the MCA-Std case. Although we have focused our analysis on the mixed Rossby-gravity wave, the differences in the model transients are not limited to this mode or to the synoptic time scales. We note that our results indicate the wave spectrum is sensitive to (i) the parameterization for convection and (ii) the location of the ITCZ. The former is demonstrated by comparing the spectra for cases that utilize different convective parameterizations but have iden-

tically located ITCZ (cf. Figs. 12a and 12d, or 12b and 12c); the latter by comparing spectra for the cases that use the same convective parameterization but realize the ITCZ in different locations (cf. Figs. 12a and 12c, or 12b and 12d).

6. The effect of the location of the ITCZ on the large-scale circulation

In this section, we examine the strength and location of the midlatitude jets in relation to the location and strength of the model ITCZs. We find that the choice of convective schemes, through their determination of the position of the ITCZ, can affect the time-mean planetary-scale circulation.

The position and speed of the jet maximum, the position of the ITCZ, and precipitation rate in the ITCZ are documented for each of the separate experiments in Table 2. The Kuo Nwv-Std, the Kuo-Poeq, and the Kuo-Flat cases are exceptional. The jets in the Kuo-Flat case are not simply related to the Hadley circulation because extraordinary and discontinuous temperature gradients exist at 30° latitude. This case is not discussed. The Kuo Nwv-Std is the only case with no zonally asymmetric waves and therefore should give approximately the same solution as Held and Hou (1980).

The Kuo Nwv-Std case has the highest jet speeds of all the cases and the jets are centered closest to the equator (Fig. 15a); the maximum jet speed is about 80% of that expected for a parcel conserving angular momentum as it traverses from the equator to the latitude of the jet core. The circulation is similar to that given by the nonlinear axisymmetric Hadley cell models of Schneider (1977) and Held and Hou (1980) [see, in particular, Held and Hou's numerical results for a nonlinear Hadley circulation with moderate vertical

diffusion ($5 \text{ m}^2 \text{ s}^{-1}$)]. Perhaps the most notable difference between the zonal-mean Kuo Nwv-Std circulation and the calculations presented in Held and Hou (1980) is the pronounced slope of the jet maximum equatorward and downward from its absolute maximum near 24° and 165 mb. Above 165–110 mb the solution produced by the CCM with westerly winds over the equator is probably dictated by the large horizontal diffusion in the stratosphere. Comparing Figs. 4 and 15a it is evident that the presence of zonally asymmetric waves decreases the amplitude of the jets and moves them poleward.

The Kuo-Poeq case, with peaked SST off and north of the equator, is exceptional as it is the only case where the model produces *one* off-equatorial convergence zone. In this case there are two jets equidistant from the equator (at 30° latitude); the jet in the Southern Hemisphere is much more intense than that in the Northern Hemisphere (Fig. 15b). This is consistent with the theory outlined by Lindzen and Hou (1988). The second, high-latitude jet found at 50°N is not predicted by Lindzen and Hou (1988), but is in accord with the observed poleward displacement of the jet in summertime.

The remaining experiments in Table 2 can be categorized into cases in which one ITCZ is found over the equator (Kuo90-Std, MCA-Std, Kuo-Peq) or two ITCZs straddle the equator (Kuo-Feb1, Kuo-Feb2, Kuo-Oct, MCA-Oct, Kuo-Std). In doing so we find that it is the *position* of the ITCZ(s) that determines the location and strength of the midlatitude jets, rather than the amount of precipitation in the ITCZ or the convective scheme that is utilized. Each of the cases that have circulations with off-equatorial ITCZs places the jet maxima at about 40° latitude, whereas each of the three cases with the ITCZ located on the equator has jet maxima located near 30°. The jet structure in

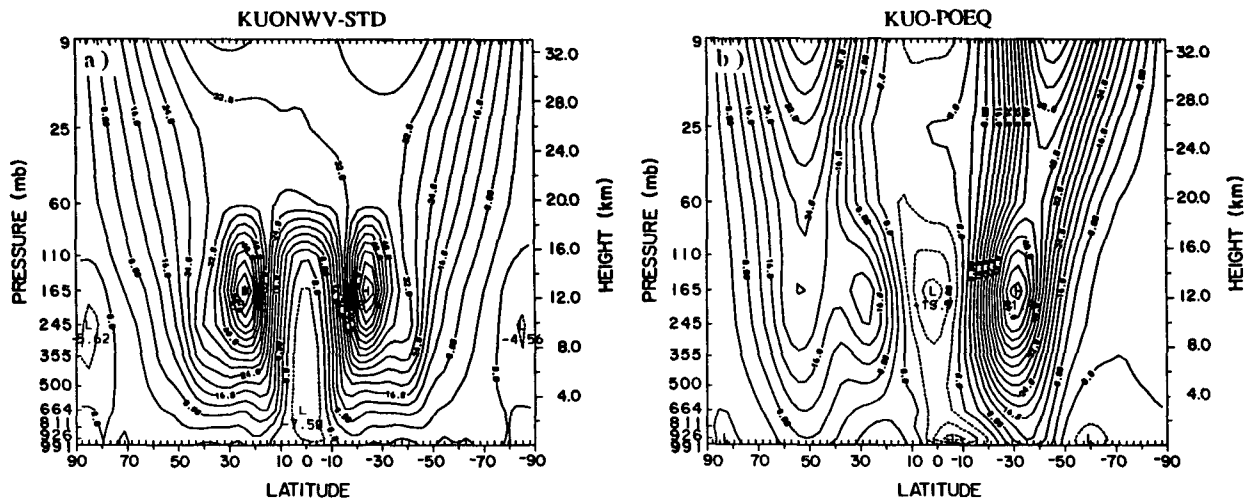


FIG. 15. A meridional cross section of the zonally averaged zonal velocity for (a) the Kuo Nwv-Std case and (b) the Kuo-Poeq case. The time averages are over 60 days. Contour interval is 4 m s^{-1} .

the single ITCZ cases is much less barotropic than those in the double ITCZ cases: the jet maximum slants downward and poleward so that in the lower troposphere the maximum winds are located near 40° in the cases with one equatorial ITCZ (e.g., Fig. 4b). The jet location is relatively insensitive to how far the ITCZ is situated from the equator, as long as it is off the equator (cf. Kuo-Feb1, Kuo-Feb2, Kuo-Oct, MCA-Oct, Kuo-Std). Furthermore, in the February cases (Kuo-Feb1, Kuo-Feb2) both Northern and Southern hemisphere jets are at the same latitude even though the precipitation is antisymmetric about the equator in both intensity and location.

The speed of the jet maximum is also dependent on the location of the ITCZ(s): the jets associated with off-equatorial ITCZs are notably stronger than those associated with the single ITCZ on the equator (the only notable exception to this is the Kuo-Std case, where the jet speeds are anomalously low in comparison with the other off-equatorial ITCZ cases). These differences can be simply understood from angular momentum considerations if the circulation cells are of equal size: an angular momentum-conserving parcel with zero angular momentum initially will acquire a larger zonal velocity if it travels from 5° to 35° than if it travels from the equator to 30° due to the increased azimuthal planetary vorticity with latitude.

Finally, the amount of precipitation (which is correlated with the magnitude of the heating and thus, the strength of the internal forcing) has little effect on the jet strength or its location (cf. the Kuo-Peq and MCA-Std cases, both of which have a single ITCZ on the equator). The Kuo-Oct and MCA-Oct cases have very similar jet structures and amplitudes, even though the convective scheme and precipitation amount is different in each case. Moreover, by comparing the Kuo90-Std case, dominated by large-scale condensation processes (see Table 2), and the MCA-Std case, characterized by convective precipitation, we note the jet structure is not affected by the *type* of dominant precipitation.

7. Discussion and conclusions

We have performed integrations with a general circulation model (NCAR CCM1) in an aqua-planet configuration, forced with symmetric equinoctial (21 March) insolation to examine the dynamics and thermodynamics associated with the intertropical convergence zones (ITCZs). The model spatial truncation is T42. The sea surface temperature (SST) is prescribed and zonally symmetric. Since the ITCZs are intimately tied to the SST and small-scale convective processes, we have performed several integrations using various SST distributions. In addition, experiments are performed using the CCM with identical prescribed SST boundary condition and solar insolation, whereby only the parameterization scheme for convection is changed.

Qualitative changes in the location of the ITCZ and in the large-scale tropical circulation are realized in the same general circulation model by employing two different parameterizations of convection: modified Kuo and moist convective adjustment. In the cases run, the model with the moist convective adjustment parameterization always forms a single ITCZ over the warmest water. By contrast, the CCM with the Kuo scheme favors a double ITCZ straddling the equator, even given a meridionally flat or "standard" SST distribution where the SST is maximum on the equator, decaying monotonically to the pole. The CCM with the Kuo scheme, however, does produce one ITCZ over the warmest water if the warmest water is flanked by very large SST gradients (the Kuo-Peq, Kuo-Poeq cases).

We have shown that, with SST maximum on the equator, zonally asymmetric motions are necessary for the model with the Kuo scheme to achieve off-equatorial ITCZs: the two off-equatorial ITCZs converge to one ITCZ onto the equator in the absence of the zonally asymmetric motions. These results are contrary to Charney (1966, 1971), whose arguments imply that the ITCZ should be off the equator even in the absence of the zonally asymmetric motions. The collapse of the two ITCZs in the Kuo-Std case to one ITCZ in the Kuo Nwv-Std case appears to be due to the reduction of transient mechanisms in the two-dimensional geometry that can efficiently organize the boundary-layer flow off the equator (see below).

We have demonstrated that the zonally propagating wave activity in the model is sensitive to the parameterization scheme for convection. For example, tropical synoptic (3–4-day) wave activity is found in each of the four model integrations. Of the four cases examined (Kuo-Std, MCA-Std, MCA-Oct, and Kuo-Peq) the structure of the activity in this band is consistent with mixed Rossby-gravity waves (Matsuno 1966) in the Kuo-Std and MCA-Oct cases. Mixed Rossby-gravity waves are not readily identifiable in either the MCA-Std case (identical to the Kuo-Std case, only employing a different convective scheme) or the Kuo-Peq case. There are other significant differences in the transients, including the intraseasonal oscillation, that appear in the twin integrations using the two convective parameterizations. The different spatial and temporal scales associated with the heating in the two schemes will likely favor the forcing of different global wave modes (see Salby and Garcia 1987; Garcia and Salby 1987).

Employing different parameterizations for convection in the CCM leads to quantitative differences in the Hadley circulation and zonally averaged subtropical jets (section 6). The sensitivity of the large-scale mean tropical circulation to the parameterization scheme for convection on the aqua planet is consistent with that documented in similar experiments with GCMs using prescribed orography and observed SST (Donner et al. 1982; Tiedtke et al. 1984; Hart et al. 1990).

The time-mean budget and distribution of moist static energy in the tropics is relatively insensitive to

the parameterization scheme for convection. However, an examination of the atmospheric columns immediately before convection occurs indicates the mechanisms that maintain the moist static energy budget in each model run are different because of inherent differences in the adjustment process for convection in the two schemes. Hence, an examination of the mean moist static energy is insufficient to evaluate a convective parameterization.

Consider the following thought experiment, based on the analysis of the conditions in the model prior to convective adjustment (section 4). Fundamental theories of the nonlinear Hadley circulation (i.e., Held and Hou 1980) suggest that an air parcel originating in the boundary layer in the divergent subtropical regions will move toward the equator to replace the air leaving the boundary layer in the rising branch of the circulation near the equator (we will not specify where). This region of rising motion must exist near the equator because of angular momentum and thermal wind constraints, even in the absence of moist convection. As the parcel flows toward the equator in the boundary layer, its moist static energy will increase due to latent and sensible heating from the surface and the flow will become convergent as it enters the rising branch of the Hadley circulation, located at approximately 12° latitude (Held and Hou 1980). Since the limiting criterion for the Kuo scheme to operate in the deep tropics is sufficient (moisture) convergence in the near-surface boundary layer (Fig. 8b), the Kuo parameterization will operate equatorward of the (transition) latitude separating the divergent and convergent boundary-layer flow. Furthermore, the Kuo scheme directly couples the lower boundary-layer flow to the upper atmosphere via a one-dimensional cloud model,² so weak perturbations of the low-level convergence in this transition region will cause convection that will easily amplify, producing a zone of enhanced convergence and precipitation—an ITCZ. Hence, in the model with the Kuo scheme the presence of sufficient transient disturbances ensures that the ITCZ will occur poleward of the region of rising motion, which would otherwise exist on the equator.

We can perform the same thought experiment assuming the physics for convection as prescribed in the MCA parameterization, which adjusts the atmosphere *locally* based on static stability. In this case, the moist static energy, which builds up within the boundary layer as air parcels move toward the equator, is occasionally vented to the atmosphere above via shallow adjustments that occur at and above the top of the boundary layer (see section 5). (Individual convective events using the MCA scheme typically span two to three layers.) However, convection immediately above the boundary layer is possible only when the ambient dry air at the

top of the boundary layer is preconditioned by transport of moist, near-surface air via lifting (convergence) throughout and above the boundary layer, which requires rather robust upward motion (see section 4b and Fig. 8e). Since, in the absence of convection, the boundary-layer circulation is organized so that the maximum upward motion will be over the warmest water (see, e.g., Schneider and Lindzen 1977; Lindzen and Nigam 1987), the preconditioning required to realize convection is also realized over the warmest water. Hence, the location of the maximum convergence (ITCZ) in the model with the MCA scheme is directly linked to the location of the warmest water.

We hypothesize, based on the analysis of the collective experiments presented, that it is only the additional degree of spatial freedom that allows two convergence zones straddling the equator on the aqua planet with a single equatorial SST maximum. Let us reexamine the thought experiment for the model with the Kuo scheme, only now we will assume an axisymmetric (two-dimensional) geometry. Our argument for off-equatorial convection involves transient disturbances causing convergence in the near-surface boundary layer. In the fully three-dimensional model, a continuum of mixed Rossby-gravity wave modes and Rossby modes exist that have long enough periods to efficiently organize the boundary-layer flow—and hence should promote CISK. Inertio-gravity modes will also be present but are too fast to organize convection (Lindzen 1974). In the axisymmetric model, however, only the $k = 0$ “mixed Rossby-gravity” mode and the inefficient $k = 0$ inertio-gravity modes are allowed; all of the Rossby waves are filtered out. The collapse of the two ITCZs in the Kuo-Std case to one ITCZ in the Kuo Nwv-Std case is consistent with a *reduction* of transient mechanisms that can efficiently organize the boundary-layer flow off the equator and away from the warmest water.

We note that Sumi (1991) has presented further results using the aqua planet model presented in Hayashi and Sumi (1986). This model, which employs a Kuo convective parameterization, produces symmetric ITCZs located 10° latitude off the equator at T42 truncation. Sumi finds that the very same model with a T21 truncation produces a single ITCZ on the equator. One plausible explanation, consistent with the foregoing hypothesis, is that the low-level convergence organized by the zonally asymmetric motions will not be resolved as well in the lower-resolution model: the convergence associated with an equatorial wave at T21 resolution will be spread over twice as large an area as that at T42. Therefore, the organization of the lower-level flow by zonally asymmetric transient motions will be much weaker in the lower-resolution model. Hence, the off-equatorial precipitation associated with these motions will be reduced significantly.

The sensitivity of the time-mean tropical circulation and ITCZ to the specific parameterization scheme for convection is one of the key results of this work. Our

² The convection due to Kuo extends throughout the depth of the troposphere in almost all instances.

results suggest the location of the time-averaged convection may be determined through a delicate balance among boundary-layer processes, the SST distribution, and the *nature* of the convective adjustment processes. The nature of convection in the model depends on the convective scheme. The tropical circulation in the model with the moist convective adjustment (MCA) scheme is strongly influenced by even weak SST gradients; with the Kuo scheme rather large SST gradients are required to change the preferred location (7° latitude) for convection. In nature, it is likely that strong SST gradients do determine the position of the ITCZ by enhancing the boundary-layer convergence over the region of maximum SST via hydrostatically induced pressure gradients (Schneider and Lindzen 1977; Lindzen and Nigam 1987; Tiedtke et al. 1988); inter-hemispheric asymmetries may also affect the position of the ITCZ. There are regions in the deep tropics, however, where SST gradients are weak enough (e.g., annually in the Indian and western Pacific oceans, and in boreal spring in the central Pacific) that SST gradients may not affect the location of the ITCZ (see Fig. 1; also Gutzler and Wood 1990). The position of the ITCZ in these regions may be determined by processes internal to the atmosphere (specifically convective and boundary-layer processes). Our results specifically indicate that in these regions the qualitative aspects of a general circulation model climatology could be quite sensitive to the parameterization of the subgrid-scale convection. Moreover, our results indicate that even when the zonal-mean tropical circulation and the location of the ITCZs are insensitive to the convective scheme (i.e., in regions of large SST gradients), the nature of the tropical transients will be highly dependent on the convective scheme.

Various investigators have reported on the global sensitivity of climate and forecast models to the parameterization scheme for convection (e.g., Donner et al. 1982; Donner 1986; Tiedtke 1984; Tiedtke et al. 1988; Hart et al. 1990). These impacts are, in general, subtle outside of the tropics. The impact of different subgrid-scale cumulus parameterizations on the *climate* of a coupled atmosphere–ocean model may not be as subtle, however. Our results indicate that the mean and transient atmospheric circulation over the tropical western and central Pacific Ocean may be very sensitive to the quantitative and subtle aspects of convection. Indeed, Tiedtke et al. (1988) noted that employing a Kuo convective parameterization in the ECMWF model resulted in a major change in the tropical 850-mb circulation. If a comparable change is registered at the surface, then the climatological wind stress and hence the SST will be affected. The variability in the climate of the tropical Pacific is dominated by the interannual ENSO phenomenon (Rasmusson and Carpenter 1982)—a phenomenon that has worldwide impacts (e.g., see Rasmusson and Wallace 1983 and references therein for an overview of the global ENSO phenomenon). The characteristics and strength of

ENSO, however, are thought to be extremely sensitive to the climatological mean atmosphere–ocean state (e.g., Battisti and Hirst 1989). Thus, an assessment of the validity of the climate simulated from a model of the coupled atmosphere–ocean system will likely require the evaluation of both the steady and transient circulation associated with the convective adjustment processes in the atmosphere and the atmospheric general circulation model.

Acknowledgments. The authors appreciate instructive conversations with Harry H. Hendon, Brant Liebmann, and Ralph Milliff. We would like to thank Chris Bretherton, Tim Dunkerton, Kerry Emanuel, David Gutzler, David Neelin, Richard Seager, Akimasa Sumi, and two anonymous reviewers for their constructive comments on an earlier version of this paper. This work was supported by the National Science Foundation (DSB and PGH; Grant ATM 8822980), the Advanced Studies Program at the National Center for Atmospheric Research (PGH), and the U.S. Navy (PR; Contract N6668568WR86062).

REFERENCES

- Anthes, R. A., 1977: A cumulus parameterization scheme utilizing a one-dimensional cloud model. *Mon. Wea. Rev.*, **105**, 270–286.
- Battisti, D. S., and A. C. Hirst, 1989: Interannual variability in a tropical atmosphere–ocean model: Influence of the basic state, ocean geometry and nonlinearity. *J. Atmos. Sci.*, **46**, 1687–1712.
- Chang, C.-P., 1973: A dynamical model of the intertropical convergence zone. *J. Atmos. Sci.*, **30**, 190–212.
- Charney, J. G., 1966: Some remaining problems in numerical weather prediction. *Advances in Numerical Weather Prediction*. The Travelers Research Center, Inc., Hartford, CT., 61–70.
- , 1971: Tropical cyclogenesis and the formation of the intertropical convergence zone. *Mathematical Problems in Geophysical Sciences. Lectures in Applied Mathematics*, 13, W. H. Reid, Ed., Amer. Mathematics Soc., 355–369.
- , 1973: Reply. *J. Atmos. Sci.*, **31**, 834–835.
- Deardorff, J. W., 1972: Parameterization of the planetary boundary layer for use in a general circulation model. *Mon. Wea. Rev.*, **100**, 93–106.
- Donner, L. J., 1986: Sensitivity of the thermal balance in a general circulation model to a parameterization for cumulus convection with radiatively interactive clouds. *J. Atmos. Sci.*, **43**, 2277–2288.
- , H.-L. Kuo, and E. J. Pitcher, 1982: The significance of thermodynamic forcing by cumulus convection in a general circulation model. *J. Atmos. Sci.*, **39**, 2159–2181.
- Dorman, C. E., and R. H. Bourke, 1979: Precipitation over the Pacific Ocean, 30°S to 60°N . *Mon. Wea. Rev.*, **107**, 896–910.
- Dunkerton, T., 1989: Nonlinear Hadley circulation driven by asymmetric differential heating. *J. Atmos. Sci.*, **46**, 956–974.
- Fraedrich, K., and M. Lutz, 1986: Zonal teleconnections and longitude–time lag correlations of the 500 mb geopotential along 50°S . *J. Atmos. Sci.*, **43**, 2116–2126.
- Garcia, R. R., and M. L. Salby, 1987: Transient response to localized episodic heating in the tropics. Part II: Far-field behavior. *J. Atmos. Sci.*, **44**, 499–530.
- Goswami, B. N., J. Shukla, E. K. Schneider, and Y. C. Sud, 1984: Study of the dynamics of the Intertropical Convergence Zone with a symmetric version of the GLAS climate model. *J. Atmos. Sci.*, **41**, 5–19.
- Gutzler, D. S., and T. M. Wood, 1990: Structure of large-scale convective anomalies over the tropical oceans. *J. Climate*, **3**, 483–496.

- Hack, J. J., L. M. Bath, G. S. Williamson, and B. A. Boville, 1989: Modifications and enhancements to the NCAR Community Climate Model (CCM1). NCAR Tech. Note, NCAR/TN-366+STR, National Center for Atmospheric Research, Boulder CO., NTRIS PB89-215594/AS, 97 pp.
- Hart, T. L., W. Bourke, B. J. McAvaney, B. W. Forgan, and J. L. McGregor, 1990: Atmospheric general circulation simulations with the BMRC global spectral model: The impact of revised physical parameterizations. *J. Climate*, **3**, 436–459.
- Hayashi, Y.-Y., and A. Sumi, 1986: The 30–40 day oscillation simulated in an “Aqua Planet” model. *J. Meteor. Soc. Japan*, **64**, 451–465.
- Held, I. M., and A. Y. Hou, 1980: Nonlinear axially symmetric circulations in a nearly inviscid atmosphere. *J. Atmos. Sci.*, **37**, 515–533.
- Hendon, H. H., and B. Liebmann, 1991: The structure and annual variation of antisymmetric fluctuations of tropical convection and their association with Rossby–gravity waves. *J. Atmos. Sci.*, **48**, 2127–2140.
- Holton, J. R., 1979: *An Introduction to Dynamic Meteorology*. Academic Press, 391 pp.
- , J. M. Wallace, and J. A. Young, 1971: On boundary layer dynamics and the ITCZ. *J. Atmos. Sci.*, **28**, 275–280.
- Jaeger, L., 1976: Monatskarten des Niederschlags für die ganze Erde. *Be. Dtsch. Wetterdienstes*, **18** (139), 38 pp.
- Krishnamurti, T. N., S. Low-Nam, and R. Pasch, 1983: Cumulus parameterization and rainfall rates II. *Mon. Wea. Rev.*, **111**, 815–828.
- Kuo, H. L., 1965: On formation and intensification of tropical cyclones through latent heat release by cumulus convection. *J. Atmos. Sci.*, **22**, 40–63.
- , 1974: Further studies of the parameterization of the influence of cumulus convection of large-scale flow. *J. Atmos. Sci.*, **31**, 1232–1240.
- Lau, N.-C., I. M. Held, and J. D. Neelin, 1988: The Madden–Julian Oscillation in an idealized general circulation model. *J. Atmos. Sci.*, **45**, 3810–3832.
- Liebmann, B. L., and H. H. Hendon, 1990: Synoptic-scale disturbances near the equator. *J. Atmos. Sci.*, **47**, 1463–1479.
- Lindzen, R. S., 1974: Wave–CISK in the tropics. *J. Atmos. Sci.*, **32**, 156–179.
- , and S. Nigam, 1987: On the role of sea surface temperature gradients in forcing low level winds and convergence in the tropics. *J. Atmos. Sci.*, **44**, 2440–2458.
- , and A. Y. Hou, 1988: Hadley circulations for zonally averaged heating centered off the equator. *J. Atmos. Sci.*, **45**, 2416–2427.
- Manabe, S., J. Smagorinsky, and R. F. Strickler, 1965: Simulated climatology of a general circulation model with a hydrologic cycle. *Mon. Wea. Rev.*, **93**, 769–799.
- Matsuno, T., 1966: Quasi-geostrophic motions in the equatorial area. *J. Meteor. Soc. Japan*, **44**, 25–42.
- Neelin, J. D., 1989: On the interpretation of the Gill model. *J. Atmos. Sci.*, **46**, 2466–2468.
- , and I. M. Held, 1987: Modeling tropical convergence based on the moist static energy budget. *Mon. Wea. Rev.*, **115**, 3–12.
- Nitta, T., Y. Nakagomi, Y. Suzuki, N. Hasegawa, and A. Kadokura, 1985: Global analysis of the lower tropospheric disturbances in the tropics during the northern summer of the FGGE year. Part I: Global features of the disturbances. *J. Meteor. Soc. Japan*, **63**, 1–19.
- Pike, A. C., 1971: Intertropical Convergence Zone studied with an interacting atmosphere and ocean model. *Mon. Wea. Rev.*, **99**, 469–477.
- Rasmusson, E. M., and T. H. Carpenter, 1982: Variations in tropical sea surface temperatures and surface wind fields associated with the Southern Oscillation and El Niño. *Mon. Wea. Rev.*, **110**, 354–384.
- , and J. M. Wallace, 1983: Meteorological aspects of the El Niño/Southern Oscillation. *Science*, **222**, 1195–1202.
- Reed, R. J., and E. E. Recker, 1971: Structure and properties of synoptic-scale wave disturbances in the equatorial western Pacific. *J. Atmos. Sci.*, **28**, 1117–1133.
- Saha, K., 1971: Mean cloud distributions over tropical oceans. *Tellus*, **23**, 183–195.
- Salby, M. L., and R. R. Garcia, 1987: Transient response to localized episodic heating in the tropics. Part I: Excitation and short-time near-field behavior. *J. Atmos. Sci.*, **44**, 458–498.
- Schneider, E. K., 1977: Axially symmetric steady-state models of the basic state for instability and climate studies. Part II. Nonlinear calculations. *J. Atmos. Sci.*, **34**, 280–296.
- , 1984: Response of the annual and zonal mean winds and temperatures to variations in the heat and momentum sources. *J. Atmos. Sci.*, **41**, 1093–1115.
- , and R. S. Lindzen, 1977: Axially symmetric steady state models of the basic state for instability and climate studies. Part I. Linear calculations. *J. Atmos. Sci.*, **34**, 263–279.
- Sumi, A., 1991: Pattern formation of convective activity over the Aqua Planet with globally uniform sea surface temperature. Part I. Effect of the rotation of the earth. *J. Meteor. Soc. Japan*, submitted.
- Swinbank, R., T. N. Palmer, and M. K. Davey, 1988: Numerical simulations of the Madden and Julian Oscillation. *J. Atmos. Sci.*, **45**, 774–788.
- Taylor, R. C., 1973: *An Atlas of Pacific Islands Rainfall*. Rep. HIG-73-9, Hawaii Institute of Geophysics, 7 pp.
- Tiedtke, M., 1984: The effect of penetrative cumulus convection on the large-scale flow in a general circulation model. *Beitr. Phys. Atmos.*, **57**, 216–239.
- , W. A. Heckley, and J. Slingo, 1988: Tropical forecasting at ECMWF: The influence of physical parameterization on the mean structure of forecasts and analyses. *Quart. J. Roy. Meteor. Soc.*, **114**, 639–664.
- Wallace, J. M., and C.-P. Chang, 1969: Spectrum analysis of large-scale wave disturbances in the tropical lower troposphere. *J. Atmos. Sci.*, **26**, 1010–1025.
- Williamson, D. L., J. T. Kiehl, V. Ramanathan, R. E. Dickinson, and J. J. Hack, 1987: Description of NCAR Community Climate Model (CCM1). NCAR Tech. Note, NCAR/TN-285+STR, National Center for Atmospheric Research, Boulder CO, 112 pp. [NTIS PB87-203782/AS.]